Sedimentary Geology 388 (2019) 81–98

Contents lists available at ScienceDirect

Sedimentary Geology

journal homepage: www.elsevier.com/locate/sedgeo

Detrital zircon geochronology reveals source-to-sink relationships in the Pearl River Mouth Basin, China

Wei Wang [a,b,c], Xianghua Yang [a,b,*], Tandis S. Bidgoli [c,**], Jiaren Ye [a,b]

[a] Key Laboratory of Tectonics and Petroleum Resources, Ministry of Education, China University of Geosciences, Wuhan 430074, China
[b] Faculty of Earth Resources, China University of Geosciences, Wuhan 430074, China
[c] Department of Geological Sciences, University of Missouri, Columbia, MO 65211, USA

ARTICLE INFO

Article history:
Received 16 January 2019
Received in revised form 8 April 2019
Accepted 9 April 2019
Available online 15 April 2019

Editor: Dr. B. Jones

Keywords:
U—Pb
Source-to-sink
South China Block
Enping Formation
Yanshanian

ABSTRACT

A major challenge in provenance and source-to-sink analysis is deciphering intrabasinal versus extrabasinal sediment sources and processes. This issue is well-illustrated by the Paleogene Pearl River Mouth Basin (PRMB), whose provenance reflects a combination of sediments eroded from the Cathaysia Block (CB), southeastern China, and from intrabasinal structural highs. Here we use new detrital zircon U—Pb ages from Paleogene formations in seven boreholes, southern PRMB, to investigate such local versus regional influences on provenance. Detrital zircons from the upper Eocene-lower Oligocene Enping Formation are dominated by Jurassic-Cretaceous ages, with a 125–110 Ma age-cluster, absent in modern river data from the CB and diagnostic of intrabasinal sediment sources. In the northern part of the basin, Mesozoic-dominated zircon age-spectra give way to Paleozoic and Precambrian grains, a pattern also recognized for the late Oligocene Zhuhai Formation, suggesting a major change in provenance likely related to extrabasinal influence from the CB. The age spectra for these samples are most similar to the northeastern Pearl River, narrowing this region as the most likely source. Spatial analysis of the results suggests that during deposition of the Enping Formation, sediment transport was not uniform and that the basin's architecture strongly influenced provenance, with structural highs acting as both sediment sources and barrier to sediment transport from the CB; whereas structural lows, with clear extrabasinal influence, functioned as sediment transport corridors. Such spatial differences are lost in samples from the Zhuhai Formation and their provenance suggests that the paleo-Pearl River and tectono-climatically driven surface processes in the CB dominated deposition thereafter.

1. Introduction

A major challenge in provenance and source-to-sink analysis is deciphering the role of intrabasinal versus extrabasinal sediment sources and processes. This issue is well-exemplified by source-to-sink systems that developed between East Asia and continental margin basins of the South China Sea during the Cenozoic. Although it is widely accepted that detritus eroded from southern China was transported to the Pearl River Mouth Basin (PRMB) (Zhao et al., 2015; Shao et al., 2016a; Liu et al., 2017; Cao et al., 2018), one of the largest offshore basins in South China Sea, during this period, the processes involved are complex given the evolving tectonics and landscape. For onshore regions (or sediment sources), topographic and drainage reorganizations associated with the India-Eurasia collision and changing climate (e.g., Clift et al., 2006, 2008; Shao et al., 2008, 2016b; Zheng et al., 2013; Zhang et al., 2017) are complicating factors that almost certainly influenced the provenance of sediments in the PRMB. For offshore regions (sediment sinks), topographic changes and related surface processes associated with episodic faulting and crustal extension and later sea-floor spreading in the South China Sea must also be accounted for (Ru and Pigott, 1986; Li et al., 1999; Wu et al., 2016).

For the PRMB, regional or extrabasinal sediments are likely to be derived from the Cathaysia Block (CB), one of two cratonal blocks that make up the South China Block on the mainland (Xu et al., 2007; Wang et al., 2013a; Fig. 1). The CB, itself, is made up of several terranes and has a complex tectonic history. Although the timing of major orogenic events and age distributions in the CB (Fig. 1A) are known (e.g., Xu et al., 2007, 2016; Wang et al., 2013a and references therein), the relative contributions of different age sources within the CB are difficult to predict from bedrock exposure areas and distributions. Several recent studies (e.g., Zhao et al., 2015; Liu et al., 2017; Wang et al., 2017) have shown that detrital zircon age signatures from modern sediments may circumvent these issues by providing datasets that better account for heterogeneities within a given catchment (e.g., zircon fertility, lithological sensitivity weathering, drainage networks effects, and mixing

* Correspondence to: X. Yang, Key Laboratory of Tectonics and Petroleum Resources, Ministry of Education, China University of Geosciences, Wuhan 430074, China.
** Corresponding author.
E-mail addresses: xhyang@cug.edu.cn (X. Yang), bidgolit@missouri.edu (T.S. Bidgoli).

https://doi.org/10.1016/j.sedgeo.2019.04.004
0037-0738/

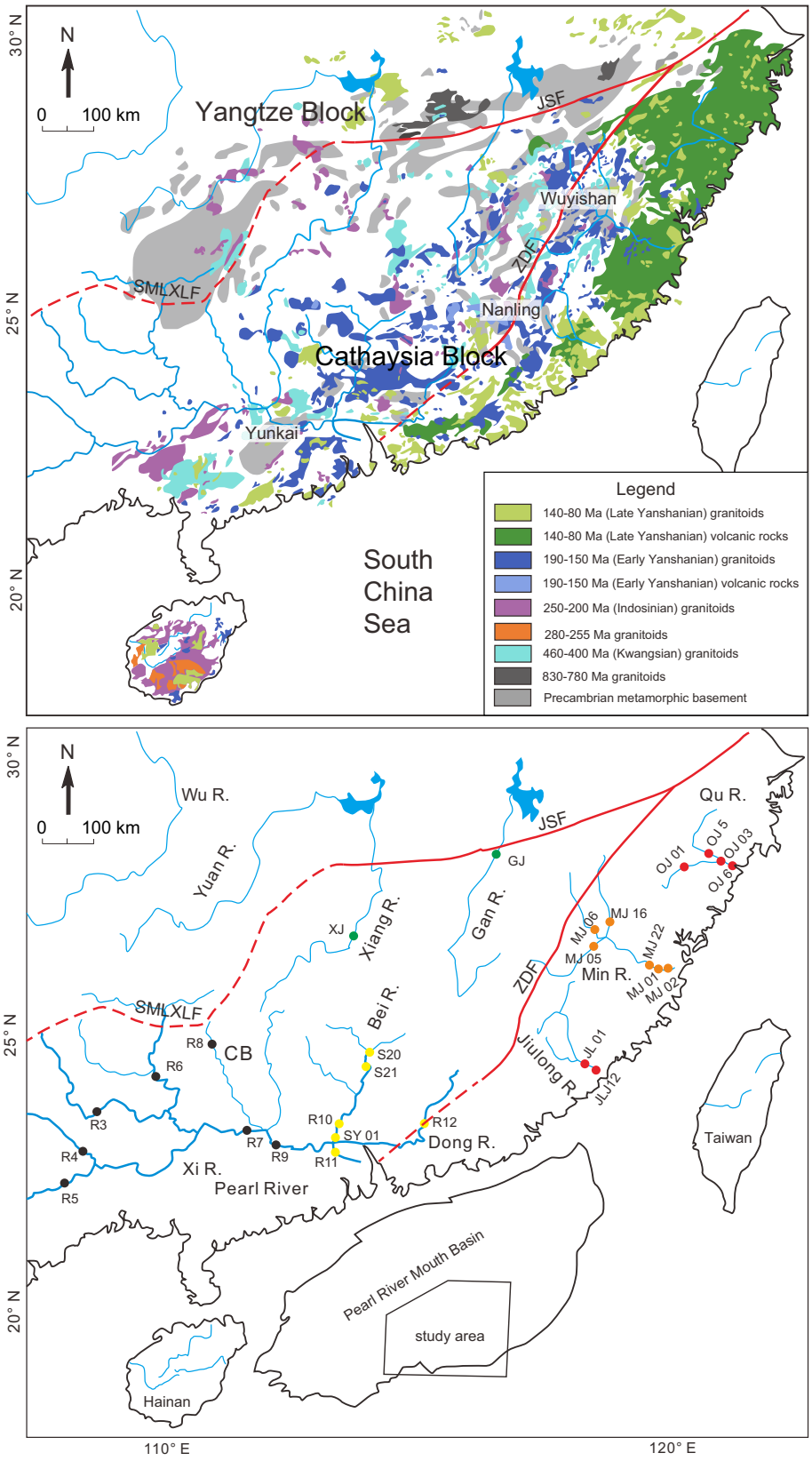

Fig. 1. (Top) Simplified geologic map of potential source areas, modified from Xu et al. (2016). The JSF (Jiang-Shao fault) and the SMLXLF (Shizong-Mile-Luoping-Xinyi-Luodian fault) are the boundaries between the Yangtze Block (YB) and Cathaysia Block (CB); the ZDF (Zhenghe-Dapu Fault) divides the Cathaysia Block into western and eastern parts (faults modified from Deng et al., 2017). (Bottom) Major rivers with published detrital zircon age samples located.

and dilution). These studies have also demonstrated the Pearl River's important role in delivering sediment to the PRMB. However, sediment contributions from rivers along the southeast coast and within the interior of the CB have been mostly ignored by the limited number of provenance studies completed to date. Given the evolving onshore landscape, a more comprehensive assessment of their role is needed.

Although drainage development and reorganization on the mainland of China are important controls on sediment delivery to the South China Sea (e.g., Clift et al., 2006, 2008; Shao et al., 2008, 2016b), recent studies suggest that intrabasinal sources and factors may also be important. Detrital zircon geochronology data from boreholes located south of Zhu 2 depression (Shao et al., 2016a), one of several sub-basins of the Pearl River Mouth Basin, suggest a similar provenance between Eocene (Wenchang Formation) and late Eocene to early Oligocene (Enping Formation) sandstones, and may point to intrabasinal sediment sources, something also suggested by ODP data from Liu et al. (2017). However, a recent investigation by Wang et al. (2017) in the Zhu 1 depression shows a profound change in the provenance of these formations, suggesting extrabasinal sediments from the South China Block entered the basin in the early Oligocene. These studies suggest that the provenance evolution of the PRMB may not be uniform, with the timing of provenance change in Zhu 1 depression, to the north, predating that of Zhu 2 depression, to the south. The relative contributions of intrabasinal versus extrabasinal sediment sources also raises important questions about the role of faults and evolving basin (sink) architecture on erosion, sediment dispersal, and provenance of sedimentary units.

In light of these challenges, this paper examines the detrital zircon provenance of Paleogene formations in seven deep boreholes distributed across the Baiyun Sag, Zhu 2 depression, in the southern PRMB. The Baiyun Sag differs from typical half-graben basins in the PRMB, in that it is a wide basin (~100 km) and contains one of thickest successions of Cenozoic sediments in the PRMB (Huang et al., 2005). Although a number of studies have focused on the Neogene history of the basin (Pang et al., 2004, 2006, 2009; Sun et al., 2014a), there has only been limited research on Paleogene syn-rift successions. We explore the role of intrabasinal versus extrabasinal sources and influences on provenance of these sediments, building on two recent investigations focused on strata to the south, near the Liwan Sag, and to the east, on Dongsha uplift (Shao et al., 2016a), and at IODP site U1435 (Liu et al., 2017). The new data, combined with data from these studies, are evaluated against a compilation of published detrital zircon geochronology data from modern rivers across the CB, which constrain potential sediment sources. Together, these datasets provide insights into the source-to-sink history of Eocene to Oligocene sediments in the PRMB and show that basin architecture and evolution exerts a strong influence on the provenance of sediments. The results also underscore the important role of the paleo-Pearl River and tectono-climatically driven surface processes in the CB on sedimentary records in the PRMB.

2. Geological setting

Cenozoic source-to-sink systems in East Asia are complex and require an understanding of the onshore and offshore geology. The onshore geology of southern China is largely made up by the South China Block, a major cratonal block with a complicated tectonic history (Wang et al., 2013a; Xu et al., 2016). The South China Block formed in the early Neoproterozoic through suturing of two Precambrian blocks: the Yangtze and CBs on northwest and southeast sides, respectively, of the Jiangshan-Shaoxing fault (Fig. 1; Xu et al., 2007; Wang et al., 2013a). The basement of the CB is composed of a Paleoproterozoic to Neoproterozoic metamorphic complex, made up by the Wuyishan, Nanling, and Yunkai terranes (Fig. 1A; Yu et al., 2010; Xu et al., 2016). In addition to Precambrian orogenic events, these terranes have been modified by three Phanerozoic events—the Kwangsian (465–400 Ma), Indosinian (270–195 Ma), and Yanshanian (190–80 Ma) orogenies—and their associated magmatism and metamorphism (Zhou et al., 2006; Wang et al., 2013a and references therein). Consequently, the lithology and geochronology of different parts of the CB vary remarkably (e.g., Li, 2000; Zhou and Li, 2000; Zhou et al., 2006; Shi et al., 2011; Wang et al., 2013a and references therein). Although clear subdivisions of the block difficult to make, geographic differences are recognizable. As shown in Fig. 1, the southeastern part of the block is characterized by Late Yanshanian (140–80 Ma) granitoids and volcanic rocks; whereas, south-central part is dominated by early Yanshanian (190–150 Ma) and Kwangsian (465–400 Ma) granitoids. The southwestern part of the block is characterized by Indosinian granitoids (270–195 Ma), Kwangsian granitoids (465–400 Ma), and a near absence of Yanshanian (190–80 Ma) terranes (Fig. 1).

The South China Sea and its associated basins make up an important part of offshore East Asia and are major sinks for sediment eroded from the south china mainland (e.g., Clift et al., 2006; Shao et al., 2016a, 2016b). The PRMB is the largest basin in the northern South China Sea, with an area of 26.68×10^4 km^2 (Shi et al., 2014). The complex Mesozoic to Cenozoic tectonic history of the basin resulted in the development of five structural zones that together comprise the PRMB. They consist of the North Uplift zone; North Depression zone, which includes the Zhu 1 and Zhu 3 depressions; Central Uplift zone, composed of the Dongsha, Panyu, and Shenhu uplifts; South Depression zone, including Zhu 2 and Chaoshan depressions; and the South Uplift zone (Fig. 2; Xie et al., 2014). Because the PRMB is formed across the continental margin, the water depth across these zones is variable, with the Zhu-1 and Zhu-3 depressions located in a shallow-water shelf setting, while the Zhu-2 depression lies along the slope near the transition to deep-water (Xie et al., 2014).

Although the underlying drivers for extension in the South China Sea remain under debate (Peltzer and Tapponnier, 1988; Li et al., 1999; Clift and Lin, 2001), the timing and progression of extensional deformation is reasonably clear. Extension initiated in the late Cretaceous to Paleocene, peaked in the Eocene, and culminated in the Oligocene to early Miocene with seafloor spreading (Ru and Pigott, 1986; Clift and Lin, 2001). The onset of the seafloor spreading in the South China Sea is diachronous, starting at around 33 Ma in the northeast and at ~23–21 Ma in the southwest, based on recent magnetic surveys and IODP (International Ocean Drilling Program) expeditions (Li et al., 2014a). In response to this tectonic evolution, four significant regional unconformities, Tg, T80, T70 and T60, developed and are recognized across the South China Sea (Figs. 2 and 3; Wu et al., 2016). It is noteworthy that in the Zhu 2 depression, the T60 boundary is tied to the Baiyun event (Pang et al., 2009) and represents migration of the shelf-slope break, from south of the Baiyun Sag to the north, and a change in depositional environments, from shallow shelf to deep water slope, with considerable subsidence (Pang et al., 2009; Shi et al., 2014).

The PRMB contains a thick succession of Cenozoic sediment that is up to 14 km thick in its deepest parts in the Baiyun Sag (Huang et al., 2005). Although the thickness and architecture of the various depressions and sub-basins differ, unconformities and stratal packages are well-correlated across the basin (Wu et al., 2016). The generalized stratigraphy of the PRMB is shown in Fig. 3. At the base of the section is the Late Cretaceous to early Eocene Shenhu Formation, which developed during the initial rifting of the PRMB. The unit is restricted to the deepest part of the Zhu 3 depression and a few sub-basins (e.g., Baiyun, Huizhou, Lufeng, and Hanjiang sags), and is dominated by the littoral lacustrine facies intercalated with volcanic rocks (Wu et al., 2016). The Wenchang Formation, deposited from the early to middle Eocene, is widespread and consists of lacustrine shales with minor sandstones, whose facies vary with position and water depth within paleo-lakes (Wu et al., 2016). The late Eocene to the early Oligocene Enping Formation varies across the PRMB. In the northern part of the basin, the formation is represented by coal-bearing terrestrial facies; however, an increasing number of researchers believe that marine transgressions may have influenced the Enping Formation in southern PRMB, particularly in the Baiyun Sag (Fu et al., 2010; Zhang et al., 2014; Wu et al., 2016). There, the Enping Formation is characterized primarily by littoral and neritic facies and scattered deltas. Paleogene deposition culminates in the PRMB with the Zhuhai Formation. This period of deposition is widely considered as transitional, with deposition of large-scale deltas fed by the paleo-Pearl River drainage to the north (Zhao et al., 2015; Shao

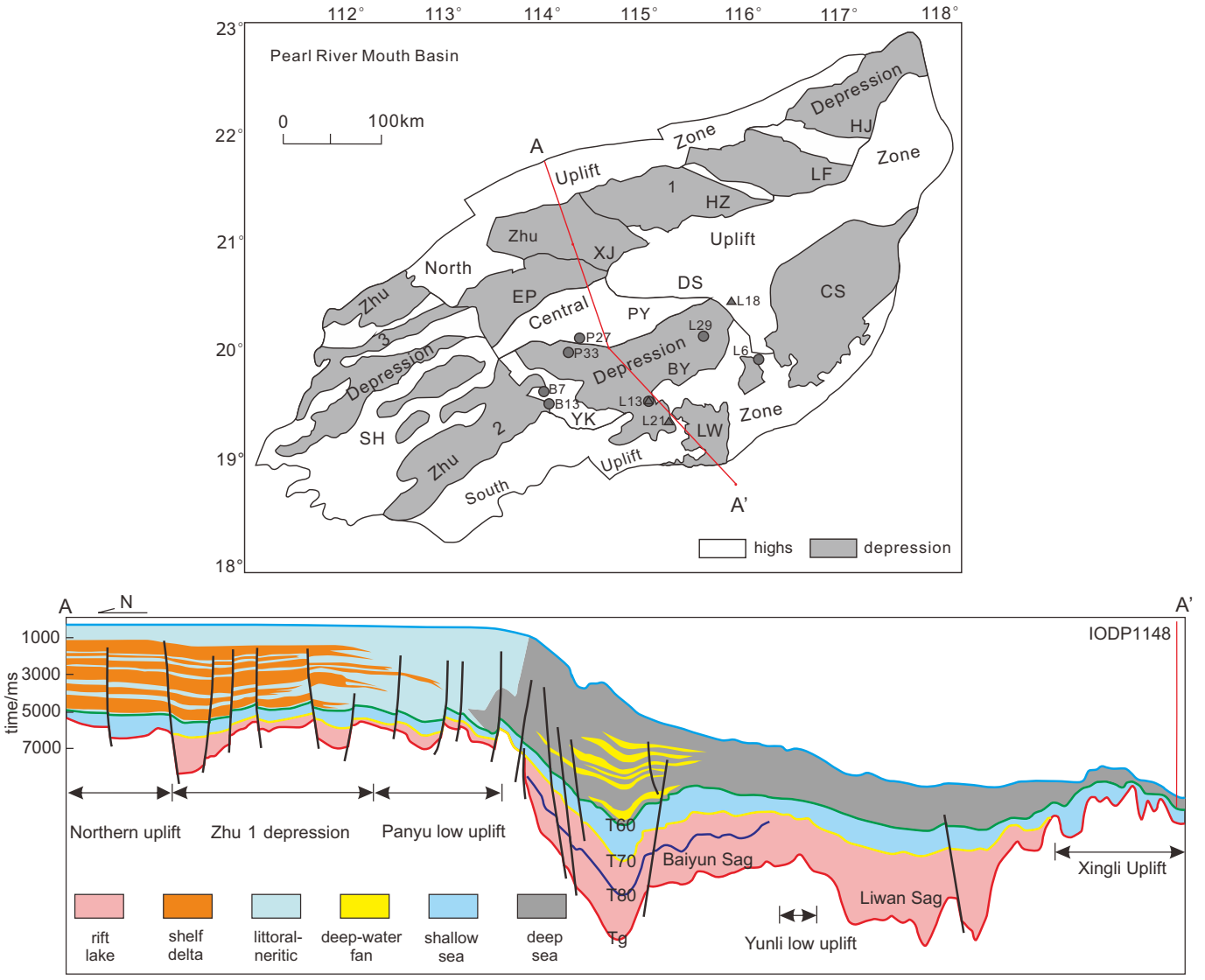

Fig. 2. Map of the major structural elements of the Pearl River Mouth Basin, modified from Xie et al. (2014). Data from Shenzhen Branch of China National Offshore Oil Corporation Ltd. Solid circles show the locations of boreholes sampled in this study. The solid triangles show the borehole sites sampled by Shao et al. (2016a). Cross section A-A′ shows the structural and facies architecture of the basin, modified from Shi et al. (2014). Abbreviation: EP = Enping Sag, XJ = Xijiang Sag, HZ = Huizhou Sag, LF = Lufeng Sag; HJ = Hanjiang Sag; BY = Baiyun Sag; CS = Chaoshan depression; LW = Liwan Sag; SH = Shenhu Uplift; PY = Panyu Low Uplift; DS = Dongsha Uplift; YK = Yunkai Uplift.

et al., 2016b). With further transgression into the Neogene, the basin became dominated by marine environments and deposition.

3. Data and methods

We collected 10 samples from seven boreholes in different parts of the Baiyun Sag: the P27, P33 are located on the Panyu low uplift and the northern edge of Baiyun Sag; the B7 and B13 boreholes were drilled into Yunkai uplift to the west; the L13 resides in the southern Baiyun Sag; and L29 and L6 in the eastern Baiyun Sag, adjacent to the Dongsha uplift (Fig. 2). Using well log data, we identified sandy intervals in each borehole to obtain cuttings from, and correlated intervals with published data using stratigraphic tops data from CNOOC (China National Offshore Oil Corporation) (Table 1). The borehole locations, sampled formations, and depths for this study and from Shao et al. (2016a), which are used for comparison and for evaluation of spatial trend, are shown in Table 1.

Fig. 4 shows the generalized stratigraphy of the sampled boreholes. Overall, the study area was dominated by marine-continental transitional deltaic and neritic sediments during the deposition of Zhuhai Formation (Chen et al., 2003; Wang et al., 2017). The sedimentary facies of Enping Formation, the primary focus of this study, are variable. The western part of Baiyun Sag, where the borehole B7 and B13 are located, is characterized by a small-scale fan delta. As illustrated by boreholes L13, L6, L21 and L29, the eastern and southern part of the basin mainly consist of small-scale braided river deltas, with obvious marine influence (Zhang et al., 2014; Wu et al., 2016; Zeng et al., 2017).

Cuttings samples were washed and then separated and concentrated using standard techniques for mechanical, heavy liquids, and electromagnetic mineral separation. Zircon grains were picked under binocular microscope, mounted in epoxy, and polished for U—Pb spot analyses. Cathodoluminescence SEM (Scanning Electron Microscopy) images were used to evaluate the internal structure of grains and identify grains that should be excluded from analysis. To avoid biasing age populations, only grains with inclusions and/or fractures that would be hard to avoid during laser spot analysis were excluded. Laser ablation-inductively coupled plasma mass spectrometry (LA-ICPMS) was carried out at the State Key Laboratory of Geological Processes and Mineral Resources.

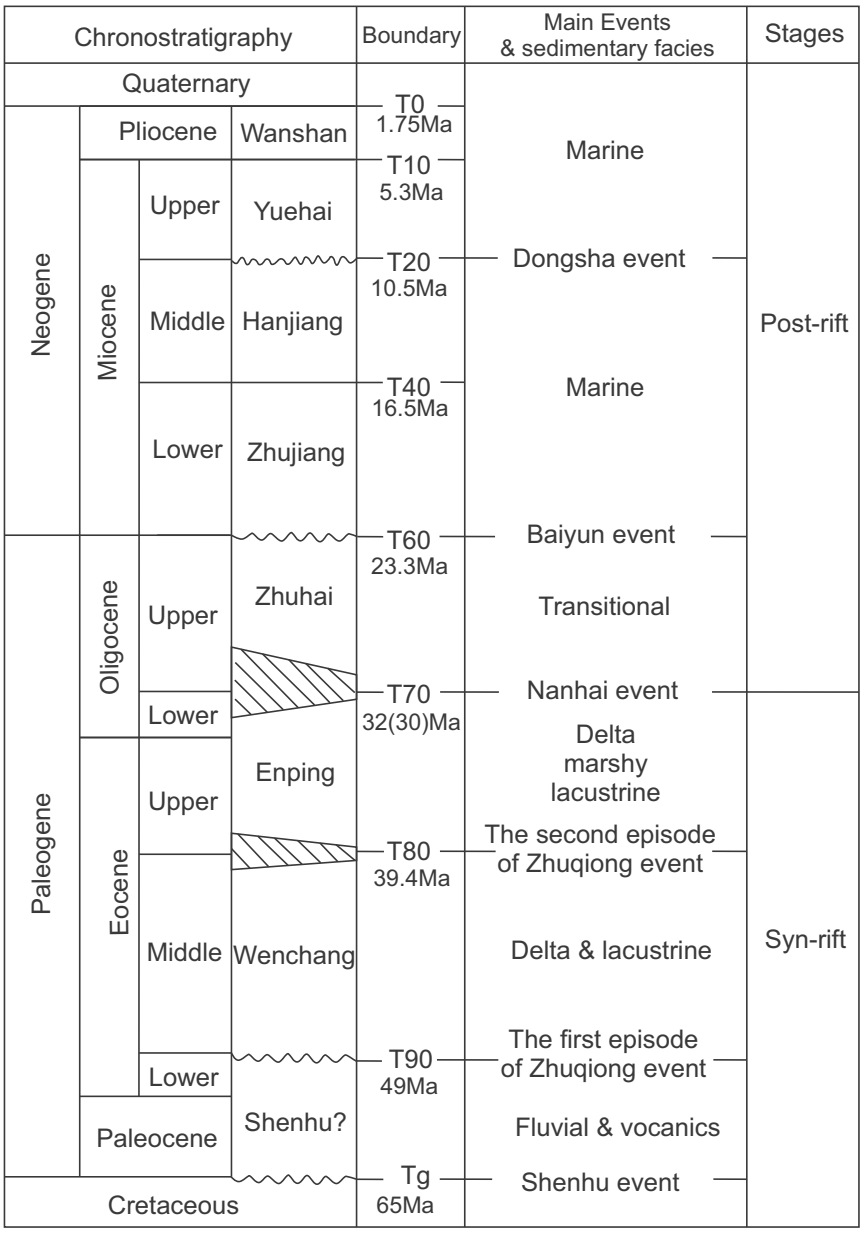

Fig. 3. Generalized Cenozoic stratigraphy, facies, and tectonic events and stages of the Pearl River Mouth Basin. Stratigraphic boundaries are major unconformities tied to several Cenozoic tectonic events (movements) (Li, 1993; Chen et al., 2003; Shi et al., 2014).

Table 1
Location, stratigraphic position, and depth of detrital zircon samples used in this study.

Location	Borehole	Formation	Interval depths (top–bottom) (m)	Concordant ages	Reference
Panyu low uplift & north slope of Baiyun Sag	P27	Enping	3680–4791	66	This study
	P33	Zhuhai	3498–3998	23	This study
		Enping	3998–5094.5	102	This study
	L29	Zhuhai	2553–2944	34	This study
Yunkai uplift	B7	Zhuhai	2642–3100	34	This study
		Enping	3100–3527	30	This study
	B13	Zhuhai	2272–2598	27	This study
		Enping	2598–2658	27	This study
Southern Baiyun Sag	L13	Enping	4482–4648	30	This study
		Zhuhai (L13 1–3)	3046–4482	303	Shao et al. (2016a)
	L21	Zhuhai (L21 1–2)	3306–3554	273	Shao et al. (2016a)
		Wenchang (L21 3–6)	3677–3961	463	Shao et al. (2016a)
Dongsha uplift	L18	Zhuhai (L18-1)	1712–1864	126	Shao et al. (2016a)
		Enping (L18-2)	1864–1884	103	Shao et al. (2016a)
	L6	Enping	2244–2292	31	This study

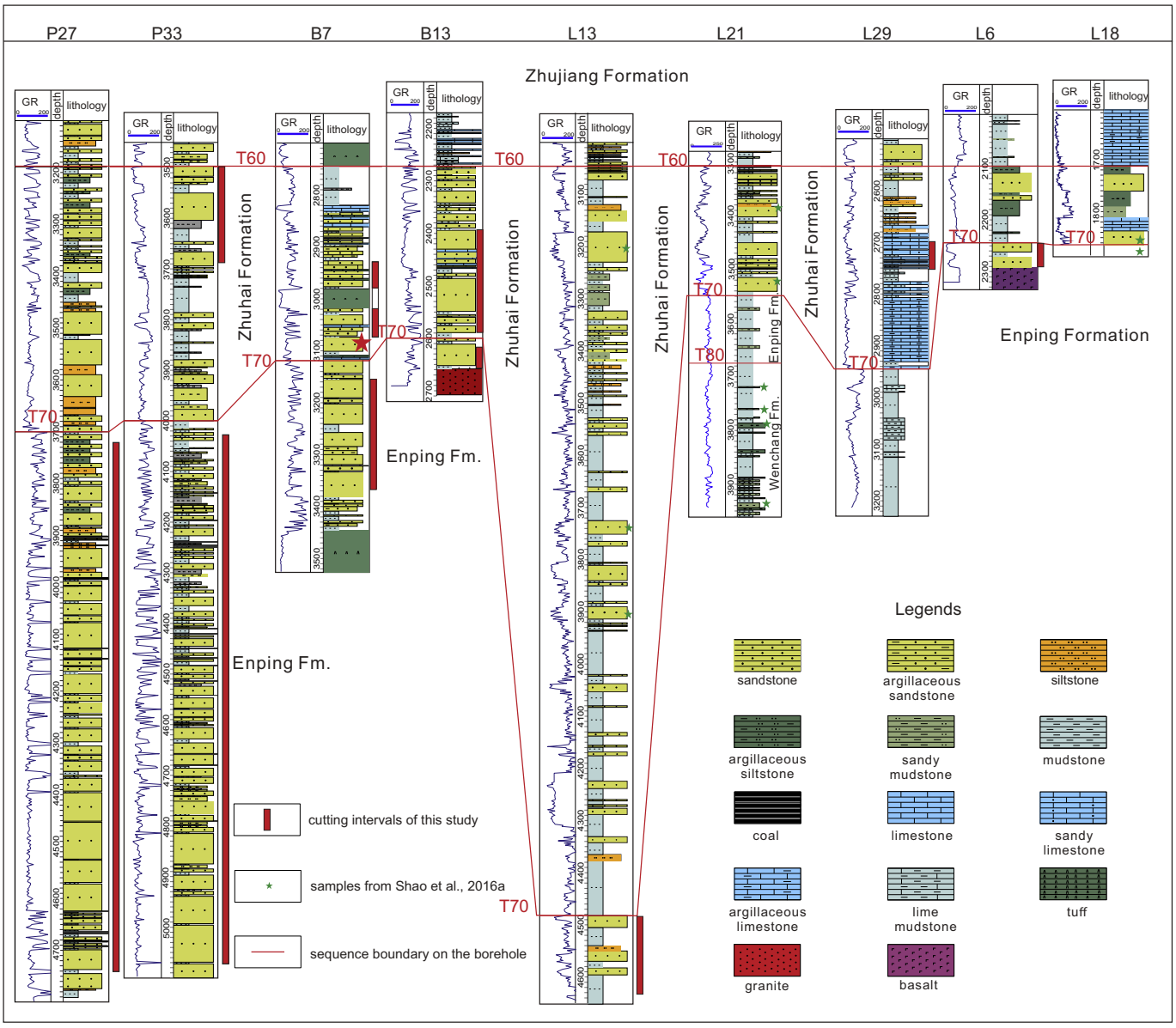

Fig. 4. Stratigraphic section showing the borehole lithologies and the positions of sequence boundaries and geochronology samples. Borehole locations are shown in Fig. 2. Well tops data are from CNOOC (China National Offshore Oil Corporation).

Laser ablation analyses were performed using a GeoLas 2005 ArF excimer laser (193 nm wavelength and ~15 ns pulse width) and the ion-signal intensities were acquired through an Agilent 7500a ICP-MS instrument. The laser energy density was 8 J/cm^2 at a frequency of 6 Hz and spot diameter of 32 μm. Helium was applied as a carrier gas with a flow rate of 0.6 L/min. Argon was utilized as the make-up gas with a flow rate of 0.78 L/min and mixed with the carrier gas via a T-connector before entering the ICP. Optimization of the gas flows was completed through ablation of NIST SRM 610 to obtain maximum signal intensity for ^{208}Pb and reduce matrix-induced interferences. The RF power is 1350 W. The plasma and auxiliary gas flow rate are 15 L/min and 1 L/min, respectively. Dwell times were set for ^{232}Th (10 ms), ^{238}U (15 ms), ^{208}Pb (15 ms), ^{204}Pb (15 ms), ^{206}Pb (20 ms), ^{207}Pb (20 ms) and ^{201}Hg (6 ms). The detector mode is dual (pulse and analog). Each analysis included ~20–30 s of background acquisition (gas blank) followed by ~50 s of data acquisition. Zircon 91500 was used as the external reference material which was analyzed twice for every eight analyses. Off-line selection and integration of background and analyte signals, and time-drift correction and quantitative calibration were conducted using software of ICPMSDataCal (Liu et al., 2010a). The mass discrimination and elemental fractionation correction was conducted using a linear interpolation (with time) according to the variations of zircon 91500. To monitor age reproducibility and instrument stability, four GJ-1 zircon standards were treated as unknowns and analyzed at the beginning and end of each run. They yielded a Concordia age of 607.5 ± 2.3 Ma (MSWD = 1.08) within 2% error range of the ID-TIMS ^{206}Pb/^{238} U age of 599.8 ± 1.7 Ma for GJ-1 (Jackson et al., 2004). More detailed LA-ICP-MS analytical procedures for the laser and mass spectrometric systems and data reduction, including uncertainty propagation, are provided by Liu et al. (2008, 2010a, 2010b). We note that alternative approaches to uncertainty propagation have been suggested by the international U—Pb geochronology community (e.g., Košler et al., 2013; Horstwood et al., 2016).

As for the "best age" cutoff between ^{207}Pb/^{206}Pb and ^{206}Pb/^{238}U ages, Spencer et al. (2016) suggest using a ~1.5 Ga cross-over point in consideration of change in chronometric power. However, all of the published detrital zircon data used in this study, from both the PRMB and the river systems in South China region (Xu et al., 2007; He et al., 2013; Xu et al.,

2014a, 2014b, 2016; Cao et al., 2015, 2018; Zhao et al., 2015; Shao et al., 2016a; Zhang et al., 2017; Wang et al., 2017), used a 1000 Ma cutoff. For consistency, we have elected to use the same cutoff as these published studies. Zircon grains older than 1000 Ma were assessed by $^{207}Pb/^{206}Pb$ ages while grains younger than 1000 Ma were determined using the more reliable concordant $^{206}Pb/^{238}U$ age (Compston et al., 1992). For zircon U—Pb ages older than 1000 Ma, the discordance was calculated based on $^{206}Pb/^{238}U$ and $^{207}Pb/^{206}Pb$ ages. For zircon ages younger than 1000 Ma, the discordance was calculated based on $^{206}Pb/^{238}U$ and $^{207}Pb/^{235}U$ ages. Although better approaches are available for establishing the discordance (e.g., Spencer et al., 2016), in this study, the detrital zircon data are mainly used for visualizing and comparing age spectra; therefore, we use a discordance filter of 10% discordance and 5% negative discordance (i.e., grains with >10% discordance or >5% reverse discordance were excluded), in agreement with the comparative datasets used (Xu et al., 2007; He et al., 2013; Xu et al., 2014a, 2014b, 2016; Cao et al., 2015, 2018; Zhao et al., 2015; Shao et al., 2016a; Zhang et al., 2017; Wang et al., 2017).

To evaluate relationships between our detrital zircon data and published datasets, we use a variety of statistical and visualization tools, routinely employed in detrital zircon provenance analysis. Age distributions are presented as histograms, pie charts, and kernel density estimation plots, which are a robust alternative for large "n" and high-precision datasets (Vermeesch, 2012; Spencer et al., 2017). Although these plots can provide insights into the provenance of a sample, direct comparison and quantitative discrimination of multiple samples is a challenge. Therefore, we also use cumulative probability plots, which reveal differences in the proportions of grains among samples (Gehrels, 2011), and multidimensional scaling analysis, which uses goodness-of-fit and closeness criteria to evaluate dissimilarities among samples (Vermeesch, 2013). Multidimensional scaling analysis quantitatively assesses these relationships using a matrix of D values from Kolmogorov-Smirnov tests to visualize or map dissimilarities in Euclidean space (Vermeesch, 2013; Spencer and Kirkland, 2016). Thus, multidimensional scaling plots will group samples with similar age spectra and separate samples that are dissimilar.

4. Results

Of the 519 detrital zircon grains analyzed, a total of 404 grains yielded ages with >10% discordance and >5% reverse discordance, with U—Pb ages ranging from 44 to 3231 Ma (Fig. 5). It should be noted that the number of grains analyzed for each sample is limited, with $n < 40$ for most samples, with the exception of boreholes in the northern part of the study area. Although larger grain populations ($n > 100$) would have been desirable to reduce potential bias in datasets and ensure that all grain-age populations are represented (e.g., Vermeesch, 2004; Andersen, 2005), acquiring adequate amounts of material, particularly from borehole cuttings in the PRMB, is a challenge. Paleogene units in the PRMB are deeply buried and boreholes into them are costly, rare, and in demand for research. That said, the age distributions appear to agree well with the published datasets, suggesting that our small grain populations adequately capture all fractions of the age distribution. These relationships are discussed in greater detail in Sections 5 and 6. Isotopic measurements and interpreted ages are provided in the data supplement (see supporting information Table S1).

Samples from the Enping Formation form two distinct groups. Samples from the P27 and P33 boreholes, located in the northern part of the study area, were drilled into thick sandstones of Enping Formation (Wang et al., 2013b; Zeng et al., 2017). The age spectra of samples from these boreholes are similar, with a wide age range from Precambrian to Cenozoic, and can be distinguished from the other Enping Formation samples (Fig. 5). The Phanerozoic ages of P27 mainly fall into three age clusters of 93–179 Ma, 231–261 Ma, and 424–459 Ma, with 6 additional grains of Precambrian age (Fig. 5). Borehole P33 shows similar Phanerozoic age groups and contains 18 Precambrian grains. In contrast, samples from the other boreholes around the Baiyun Sag are dominated by Mesozoic grains, although the age distributions vary within Mesozoic clusters (Fig. 5). The age ranges for B7 and B13 boreholes, drilled into the Yunkai uplift, are narrow, mainly from Mesozoic-age sources that fall into two groups: a 104–168 Ma group with a peak at 159 Ma and a 229–259 Ma group with a peak at 238 Ma. For borehole B13, 24 of the total 27 concordant ages fall into the range of 100–110 Ma, with three slightly older grains of 117 Ma, 123 Ma, and 155 Ma. Mesozoic grains also dominate in the southern part of the study area, where 30 concordant ages from borehole L13 show a major peak at 116 Ma and a weak peak at 251 Ma. The Enping Formation sample from borehole L6, drilled south of Dongsha Uplift, near the eastern margin of the Baiyun Sag, has a major Mesozoic age cluster that ranges from 106 to 240 Ma (25 of 31 grains) and four Precambrian grains.

Only 4 samples, from boreholes P33 to the north, L29 to the northeast, and B7 and B13 on the Yunkai uplift, were analyzed from the Zhuhai Formation. The samples had limited numbers of grains, but nonetheless show some distinct trends. As shown in Fig. 5, the P33 and L29 boreholes in the northern and northeastern parts of Baiyun Sag have wide age ranges and high proportions of Precambrian grains. The sample from borehole B7, near the western margin of the sag, also shows a wide age range and a clear Kwangsian age peak that accounts for 45% (15 of 34) of the total grains. For the B13 borehole sample, Indosinian and Kwangsian zircon grains appear, but the age spectrum is still dominated by Yanshanian grains with a narrow age range (117–97 Ma). Overall, the Zhuhai Formation shows more Precambrian-Paleozoic grains than the Mesozoic-dominated Enping Formation, a trend that is also observed in published data from the L21 and L13 boreholes by Shao et al., (2016a) (Fig. 5).

5. Interpretation

5.1. Detrital zircon geochronology of potential sediment source regions

To better characterize potential sediment source regions, we compiled published detrital zircon U—Pb ages from six major rivers that cross the CB (Fig. 1). The CB covers the bulk of southeast China and is the most likely sediment source for the northern margin of the South China Sea (Shao et al., 2016a; Liu et al., 2017; Wang et al., 2017). In addition to these rivers on the mainland of China, we also summarize data from two other potential source areas: Hainan Island and intrabasinal source regions within the PRMB (Fig. 1). We exclude the Yangtze Block as a potential sediment source based on observations from both bedrock and detrital zircon geochronology that show the block is dominated by Precambrian zircons with a notable Neoproterozoic age cluster (He et al., 2013; Zhang et al., 2017) that is absent or rare in the sedimentary rocks in the PRMB.

The compiled data are summarized in Fig. 6 and show that sediment from major rivers across the CB have distinct detrital zircon age distributions. Sediments from the Min River, in the east-central CB, and the Xiang and Gan rivers, in the northern CB, have pronounced Kwangsian age peaks and large numbers of Precambrian grains that are absent or depressed in other river samples. These rivers also have an early Yanshanian-age peak that is also prominent in samples of the northeastern Pearl River, in the south-central CB, and Ou and Juilong rivers, along the southeast coast. The northeastern Pearl River and rivers on Hainan Island also have notable late Yanshanian age peaks. In contrast, the western Pearl River in western CB is noted for its strong Indosinian and Precambrian age peaks and near absence of Yanshanian ages. In the following sections, we provide more detailed descriptions of catchments and detrital zircon age distributions.

5.1.1. Ou and Jiulong rivers (southeast coast)

The southeast coast of Cathaysia can be characterized by catchments of the Ou and Jiulong rivers, east of Zhenghe-Dapu Fault (Fig. 1A). Data

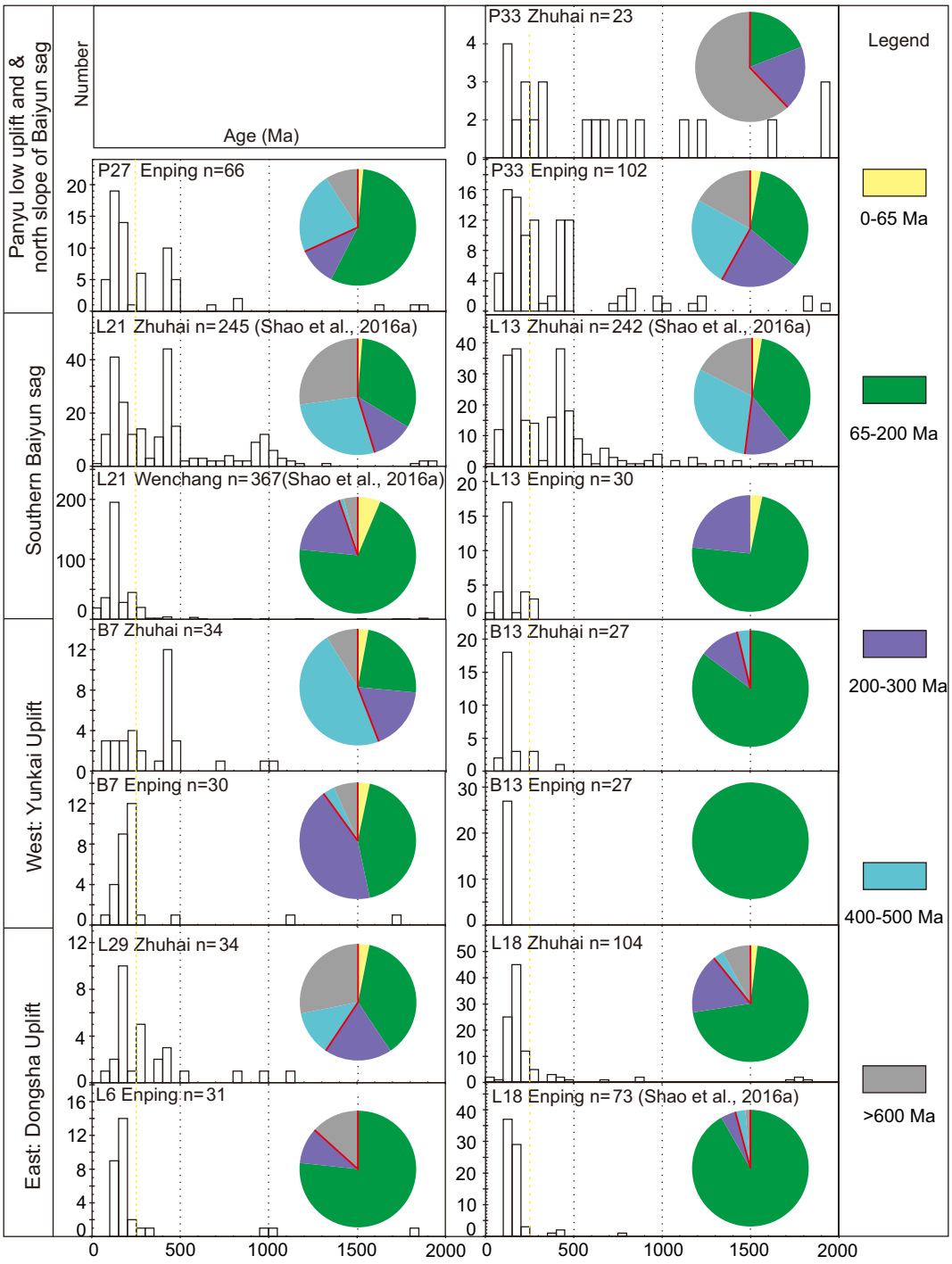

Fig. 5. Histogram plot (50 Ma bin size), probability density distribution, and pie charts of the zircon U—Pb ages of samples in this study and Shao et al. (2016a). The samples and data are divided into four geographic regions: (1) the northern group includes the Panyu low uplift and the northern slope of Baiyun Sag; (2) the western group in made up by the Yunkai uplift; (3) the southern group is the southern Baiyun Sag; and (4) the eastern group comes from Dongsha uplift. Grains with ages >2000 Ma are not shown in the figures because of the extreme single value in each sample would shrink the plot scales.

from Xu et al. (2007) demonstrate the age spectrum of the Ou river is dominated by late Yanshanian-stage (140–80 Ma) zircons, with a small number of Paleoproterozoic grains that may imply influence from ancient metamorphic basement, likely exposed in Wuyi or Nanling terrain (Fig. 6A, Xu et al., 2007). In addition to these peaks, the Jiulong River is characterized by a small number of early Yanshanian (190–150 Ma) and Indosinian grains (270–195 Ma) (Fig. 1B) that likely reflect sporadic exposures of granitoids at the headwaters of the river (Fig. 6B, Xu et al., 2014a; Zhang et al., 2017). However, Kwangsian grains (465–400 Ma) are almost absent in the southeast coast.

5.1.2. Min River (east-central CB)

The Min River resides between drainages of the Ou and Jiulong rivers, along the southeast coast of China. The upstream reaches of the river flow through Precambrian basement of the Wuyishan terrane, made up by the Paleoproterozoic Badu Complex (1890–1830 Ma), some of the oldest basement in the CB (Yu et al., 2012; Fig. 1A). Kwangsian granitoids (465–400 Ma) are also developed within the terrane (Wang et al., 2013a and references therein; Fig. 1A). The Min River drainage basin also crosses major Yanshanian igneous belts (Xu et al., 2014a, 2016). As a result, the age spectrum of

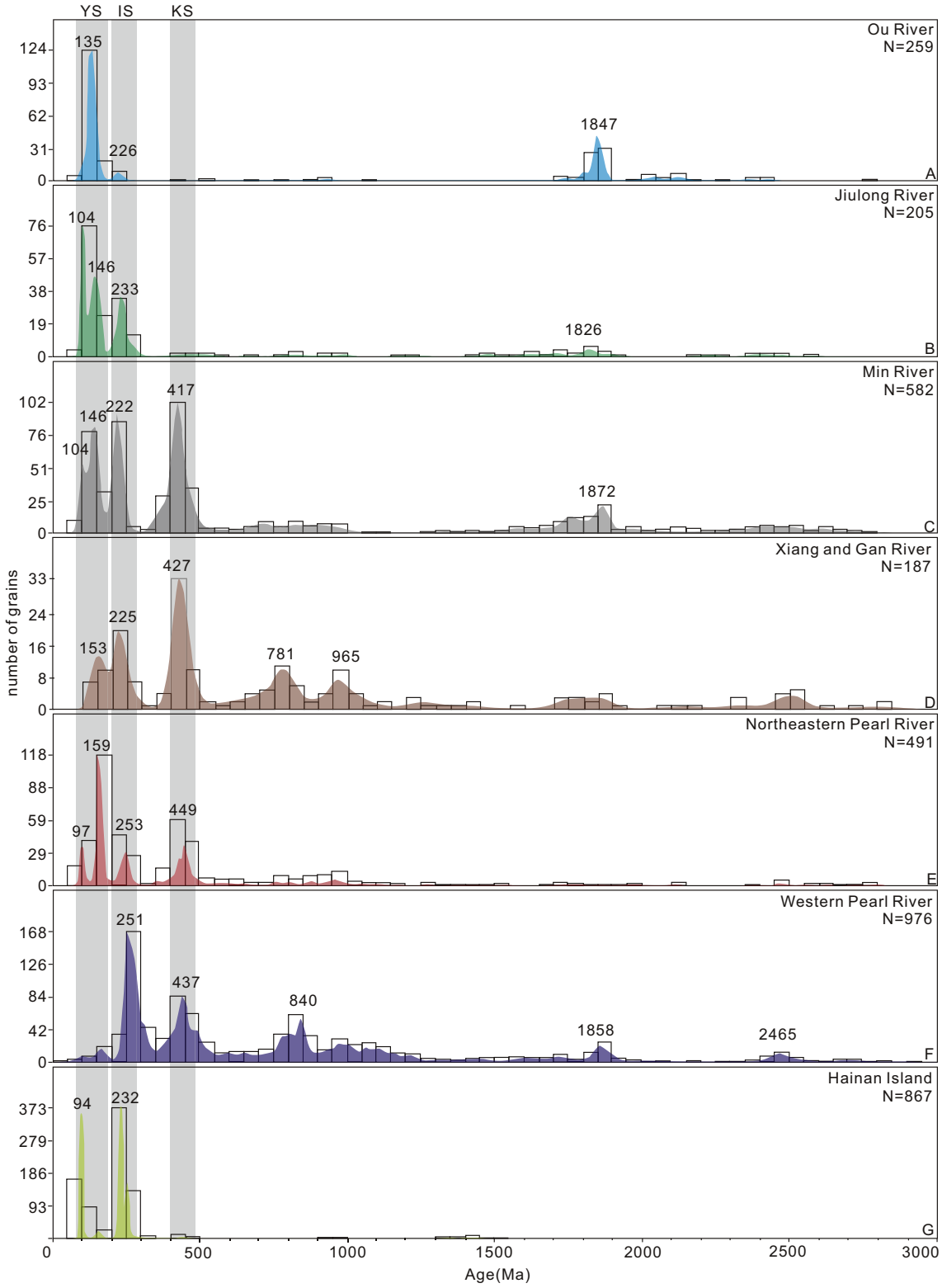

Fig. 6. Kernel density estimation plots for zircon U–Pb ages of modern river sediment from the east China mainland and Hainan Island. Data for the Pearl River is from Zhao et al. (2015) and Xu et al. (2007); Ou River is from Xu et al. (2007); Min River is from Xu et al. (2014a, 2016) and Zhang et al. (2017); Jiulong River is from Zhang et al. (2017) and Xu et al. (2014a); Xiang and Gan River are from He et al. (2013); Hainan Island is from Xu et al. (2014b), Cao et al. (2015), and Wang et al. (2015). Abbreviation: KS—Kwangsian (465–400 Ma); IS—Indosinian (270–195 Ma), YS—Yanshanian (190–80 Ma).

Min River is complicated, with Paleoproterozoic, Kwangsian (465–400 Ma), Indosinian (270–195 Ma), and early (190–150 Ma) to late Yanshanian (140–80 Ma) age clusters (Fig. 6C, Xu et al., 2014a, 2016; Zhang et al., 2017).

5.1.3. Xiang and Gan rivers (northern CB)

The Xiang and Gan rivers flow through the northern CB, near its boundary with the Yangtze block. The two rivers transect a region made up of Precambrian metamorphic basement and sporadic

Indosinian granitoids intrusions (Fig. 1A). The age spectrum from modern sediment from these rivers, which represent the northern CB, show major peaks of Kwangsian (465–400 Ma) and Indosinian age (250–200 Ma) (Fig. 6D, He et al., 2013). Additionally, two Neoproterozoic peaks are also recognized and may imply influence from the Yangtze Block to the north (He et al., 2013; Deng et al., 2017; Zhang et al., 2017, Fig. 6D).

5.1.4. Pearl River (central and western CB)

The Pearl River system includes watersheds of the Xi (West), Bei (North), and Dong (East) rivers. Several studies have evaluated the large and variable drainage area (e.g., Xu et al., 2007; Zhao et al., 2015; Liu et al., 2017). The data provided by these studies show that the river's drainage may be divided into two parts based on its western (Xi River) and northeastern (Bei and Dong rivers) tributaries (Shao et al., 2016a).

The northeastern Pearl River drainage, in the south-central part of the CB, mainly flows across Yanshanian age igneous rocks and Indosinian and Kwangsian granitoids (Zhao et al., 2015; Fig. 1). The age spectrum is characterized by a major early Yanshanian peak (190–150 Ma) and two subordinate clusters corresponding to the age ranges for the Kwangsian (465–400 Ma) and Indosinian orogenies (270–195 Ma) (Xu et al., 2007; Zhao et al., 2015, Fig. 6E).

The western part of Pearl River (Western CB) flows through the Yangtze Block to the northwest and Yunkai terrane to the south, where large exposures of Kwangsian (465–400 Ma) and Indosinian granitoids (270–195 Ma) are present. Compared with the northeastern part of the river, the age distribution is more complicated, with large Indosinian and Kwangsian age peaks and a near absence of Yanshanian-stage (190–80 Ma) grains (Fig. 6F, Zhao et al., 2015). It should be noted that a Neoproterozoic peak is also present in the age spectra and may be the signature of Yangtze Block located to the northwest (Zhao et al., 2015).

5.1.5. Hainan Island

Hainan Island, located in the western part of the northern South China Sea, is considered one of the main source areas for sediment to Yinggehai and Qiongdongnan basins (Cao et al., 2015; Jiang et al., 2015). The PRMB lies to the east of Hainan Island, but the island is seldom considered as a provenance area for the PRMB because of the relatively long distance between the two. Linkages between the island and the PRMB have also been hindered by limited research on the eastern part of the basin.

The geology of Hainan Island is complex, with evidence for Precambrian to Cenozoic tectonomagmatism; however, the bedrock of the island is made up dominantly of Indosinian and Yanshanian igneous rocks that form two main age clusters of 280–210 Ma and 110–90 Ma (Xu et al., 2014b; Cao et al., 2015; Wang et al., 2015; Fig. 6G). This bimodal age distribution is well recorded by the modern sediment from island from the Lingshui and Wanquan rivers (Cao et al., 2015); Zhubi, Changhua, Beili, Ganen, Wanglou and Ningyuan rivers (Wang et al., 2015), and beaches along Yalong Bay (Xu et al., 2014b) (Fig. 6G).

5.1.6. Intrabasinal sediment sources

In addition to the regional or extrabasinal provenance, local structural highs within the PRMB could be a significant source for sediment, particularly during the syn-rift period (Shao et al., 2016a; Liu et al., 2017; Wang et al., 2017). Although the lithology and geochronology of local sediment sources is difficult to characterize and remains controversial (e.g., Li et al., 1998; Sun et al., 2014b; Shao et al., 2016a), limited borehole data indicate that structural highs in the central PRMB are dominated by Jurassic and Cretaceous granites with U—Pb ages ranging from 102 to 162 Ma (Shi et al., 2011; Wu et al., 2016). Eocene syn-rift sediment from both the Zhu 1 depression (Wang et al., 2017) to the north and IODP site U1435 (Liu et al., 2017) to the south are interpreted as being sourced from intrabasinal basement uplifts, dominated by Yanshanian (190–80 Ma) igneous rocks.

5.2. Spatial and temporal provenance trends in the Baiyun Sag

To evaluate temporal and spatial trends in provenance across the Baiyun Sag, we sorted the detrital zircon data from this study and from Shao et al. (2016a) by formation and by geographic position (Fig. 5). Shao et al. (2016a) focused on several boreholes in the South China Sea, located to the south and east of the study area, near the Liwan Sag and on the Dongsha uplift, and provides one of only a few detrital zircon datasets that our results can be evaluated against. So that direct comparisons can be made between these two datasets, we used regional unconformities and well tops data from CNOOC to organize the data from Shao et al. (2016a) in stratigraphic formations (i.e., Wenchang, Enping and Zhuhai formations) (Table 1).

5.2.1. Eocene Wenchang Formation

Due to the significant burial depth of the Zhu 2 depression and Baiyun Sag, boreholes drilled into the Wenchang Formation are rare. Although we were unable to sample the Wenchang Formation in this study, Shao et al. (2016a) acquired 4 samples from borehole L21 (L21-3 to L21-6) that belong to Wenchang Formation, and from these obtained 367 concordant ages. The age spectra from these samples, shown in Figs. 5 and 7, are dominated by a Yanshanian (190–80 Ma) age cluster, with a peak at 114 Ma, and a small peak at 232 Ma. Visually, the age pattern is similar with the Wenchang Formation from Zhu 1 depression to the north (Fig. 7A) (Wang et al., 2017) and to Eocene samples from IODP Site U1435 to the south in the South China Sea (Liu et al., 2017) (Fig. 7B) and suggests a similar source for all three sites.

5.2.2. Eocene-Oligocene Enping Formation

By comparison to the Wenchang Formation, the Enping Formation is well sampled in the study area. The age distributions in Fig. 5 show that Enping Formation samples have a major peak between 180 and 90 Ma, suggesting significant influence from Yanshanian magmatic rocks. Most of the samples also show a small age peak from 195 to 250 Ma that corresponds with the timing of the Indosinian orogeny (195–270 Ma). Visual inspection of the kernel density estimations plots in Fig. 7 suggests the most of the Enping Formation samples from the study area, with their Mesozoic-dominated age spectra, are similar to the Wenchang Formation in the L21 borehole, as well as to Eocene samples from Zhu 1 depression and from IODP site U1435. In contrast, the age distributions for samples from boreholes in the northern part of the study area (P27 and P33) are differentiated from the other Enping Formation samples by a pronounced Paleozoic age peak that corresponds with the timing of the Kwangsian orogeny (400–465 Ma) and a greater number of Precambrian zircons, which together point to a different source area (Fig. 7).

5.2.3. Oligocene Zhuhai Formation

A significant change in age spectra occurs between the Enping and Zhuhai formations that is recognized across the study area and is clearly illustrated by the age distributions for individual samples (Fig. 5). The pronounced Kwangsian peak in the B7 borehole in the west and recognized in detrital zircon data from the L13 and L21 boreholes in the south are similar. The Mesozoic-dominated age pattern gives way to Paleozoic-Precambrian-dominated age distributions that are particularly noticeable for samples in the southern part of the study area (Figs. 5 and 7). Although samples from the boreholes L13 and L18 are still dominated by Mesozoic grains, there is an obvious change in the age spectra, with a greater number of old (>250 Ma) grains present. These observations paired with an expansion of neritic facies during the deposition of Zhuhai Formation, support earlier interpretations that the whole of the PRMB became connected at this time and may have shared a similar source area (Chen et al., 2003; Zhao et al., 2015; Shao et al., 2016a). In Fig. 7F, we aggregate the data from Zhuhai Formation into a single KDE plot. The age peaks in this view are similar to the northern Enping Formation and may point to a similar source for sediments.

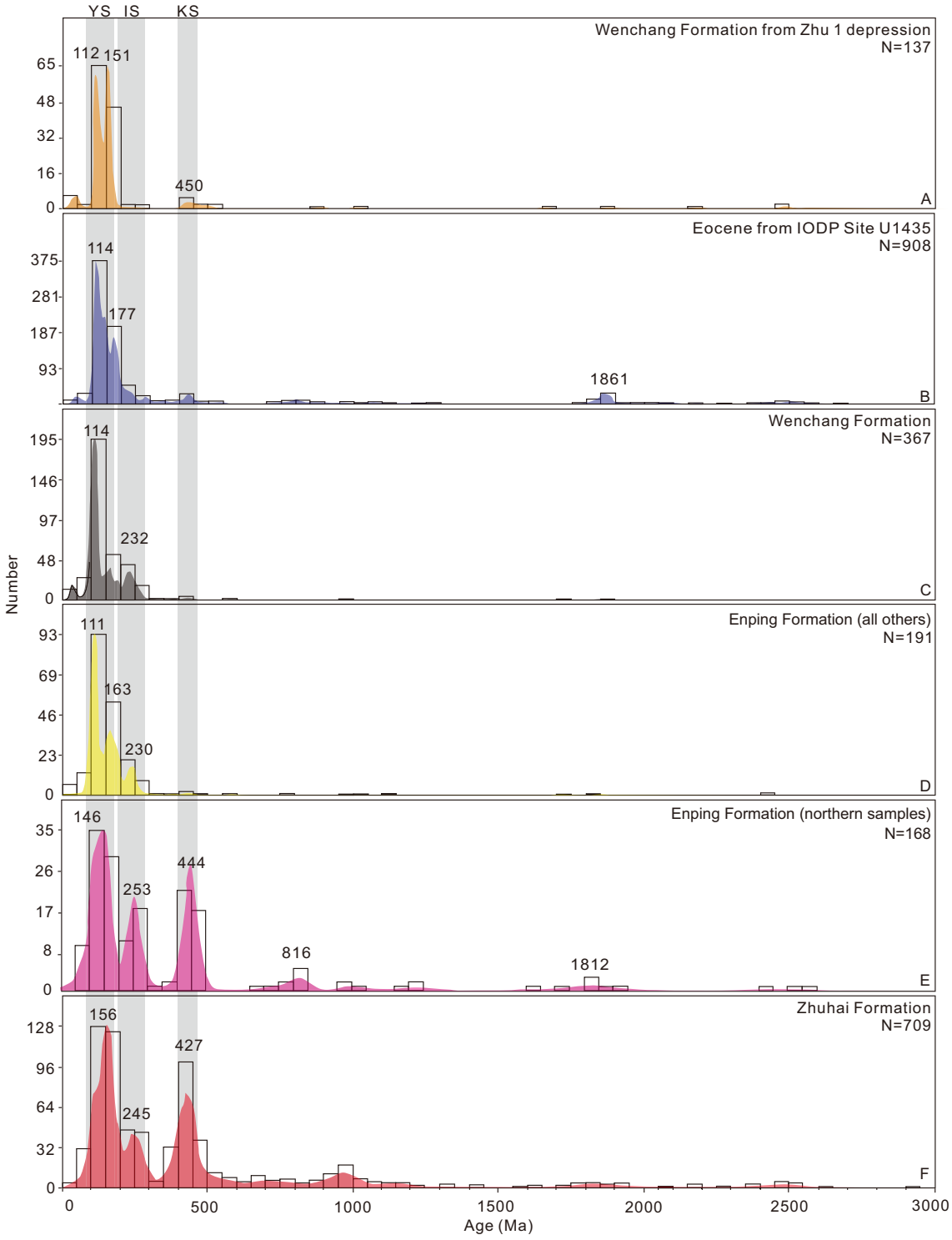

Fig. 7. Kernel density estimation (Vermeesch, 2012) and histogram plots (50 Ma bin size) for (A) Eocene samples from Zhu 1 depression (Wenchang Formation), (B) IODP Site U1435 (Liu et al., 2017), (C) Enping Formation, excluding northern samples, (D) northern Enping Formation samples, and (E) Zhuhai Formation.

Similarities between distributions of Wenchang, Enping and Zhuhai formations from different parts of the Baiyun Sag were also assessed by the Kolmogorov–Smirnov (K–S) method (Vermeesch, 2013). We calculated the parameter of V_{K-S} following Malusà et al. (2013, 2016), where if $V_{K-S} > 0$, differences between distributions lack statistical significance. The results show that all of the samples fail the test (Fig. 8), indicating that until deposition of Zhuhai Formation, the provenance around the Baiyun Sag was undergoing significant changes.

5.3. Source-to-sink relations

In order to evaluate relationships between the modern river data, which represent the potential sources, and the data from the PRMB (sink), we compare age distributions using visual and statistical methods. Visual comparisons of the data are made using kernel density estimation and cumulative age probability plots, whereas statistical comparisons are made through multidimensional scaling analysis.

Fig. 8. Similarity between age distributions of Wenchang, Enping and Zhuhai samples from the same borehole (P33 in the north, L21, L13 in the south, B7, B13 in the west and L18 in the east) are evaluated by the K–S method, comparing the maximal distance between cumulative frequency curves with the critical value for a 0.05 significance level. The detailed calculation of V_{K-S} follows Malusà et al. (2013, 2016). Where if $V_{K-S} > 0$, differences between distributions are statistically not significant.

The detrital zircon age data for the Enping Formation suggests that samples may be divided into two different spatial groups, with different age distributions and potential provenance. Kernel density estimation plots show that the most of the Enping Formation samples from the study area, with their Mesozoic-dominated age spectra (Fig. 7D), are similar to the Wenchang Formation in the L21 borehole (Fig. 7C), as well as to Eocene samples from Zhu 1 depression (Fig. 7A) and from IODP site U1435 (Fig. 7B). The age spectra are also similar to those of modern sediment from the Ou and Jiulong rivers (Fig. 7A–B). In contrast, the northern Enping Formation and Zhuhai samples, with three Phanerozoic age clusters (465–400, 270–195, and 190–80 Ma) (Fig. 7E), are most similar to the Min River (Fig. 6C) and northeastern Pearl River age spectra (Fig. 6E).

Fig. 9 compares the zircon data from the study area (same data in Fig. 7) with modern river sediment from candidate source areas (same data in Fig. 6) in CB, samples from Wenchang Formation in Zhu 1 depression (Wang et al., 2017), and samples from IODP site U1435 (Liu et al., 2017). It is clear from the cumulative age probability plots, the Xiang and Gan River have a close relationship with the western Pearl River samples, and are distinguished from the other source regions and samples by an absence of Yanshanian-age grains and the inclusion of Neoproterozoic grains. These characteristics are a distinguishable feature of Yangtze Block (He et al., 2013; Zhang et al., 2017), for which the Xiang and Gan River are adjacent to and the northernmost reaches of the Western Pearl River flows across. These relationships are also revealed in the multidimensional scaling plot (Fig. 10), which shows a close relationship between these samples and precludes the possibility that these river's drainages served as major source areas for the Zhu 2 depression.

From the cumulative age probability plots, it can also be seen that the Zhuhai Formation (red solid line) and northern Enping Formation (pink solid line) parallel one another and are most similar to the northeastern Pearl River samples (red dash line). These three are also well grouped in the multidimensional scaling plot (Fig. 10), suggesting strong affinity among them. Fig. 9 also shows that the Wenchang Formation (black solid line) and other Enping Formation (yellow solid line) samples (B7, B13, L6, L13 and L18) from the study area appear most similar to and have a close relationship with the Wenchang Formation samples from the Zhu 1 depression (orange line) and from IODP site U1435 (dark blue solid line). The figure also demonstrates that, despite some similarities in the kernel density estimation plots, all of these samples are poorly aligned with the modern river samples, including samples from the southeast coast of the CB, which are dominated by Yanshanian-stage magmatism (Figs. 9, 10).

Multidimensional scaling analysis further illustrates the above relationships. Fig. 10 show that the Enping Formation in the northern part of the study area has a close relationship with the Zhuhai Formation, and both are most similar to the detrital zircon data from the northeastern Pearl River in the CB. In contrast, the age spectra for the Wenchang Formation and Enping Formation elsewhere in study area are far from the detrital zircon data from CB rivers and Hainan Island, but are closest to samples of the Wenchang Formation in the Zhu 1 depression (Wang et al., 2017) and from IODP U1435 (Liu et al., 2017), which are interpreted as derived from local intrabasinal sediment sources (Figs. 9 and 10).

6. Discussion

Our analysis and interpretation show that from deposition of the Wenchang to Enping to Zhuhai Formation, detrital zircon age distributions change from Yanshanian-dominated (190–80 Ma) to including increasing numbers of Kwangsian (465–400 Ma) and Precambrian grains, suggesting a major change in provenance that may be related to evolving surface processes and landscape during the Oligocene. The Yanshanian grains that dominate the Wenchang and southern Enping Formation samples have two potential sources that must be considered: (1) the change in provenance could be the result of reorganization of drainages that fed the basin from southeast coast to the interior of CB or (2) the change could reflect a switch in provenance from intrabasinal sediment sources to extrabasinal sediments from the CB. In the following sections, we explore these possibilities and their implications.

6.1. Yanshanian magmatism and intrabasinal sediment sources

Yanshanian (190–80 Ma) zircon grains make up major age peaks in samples from the Ou, Min, Jiulong, and northeast Pearl rivers; major rivers in Hainan Island; Wenchang Formation in Zhu 1 depression and borehole L21; Eocene samples from IODP Site U1435; and the Enping and Zhuhai samples in this study. As shown in the Fig. 11, there are large differences in Yanshanian zircons from modern river sediment in potential source areas of the CB and the target strata in the PRMB, that

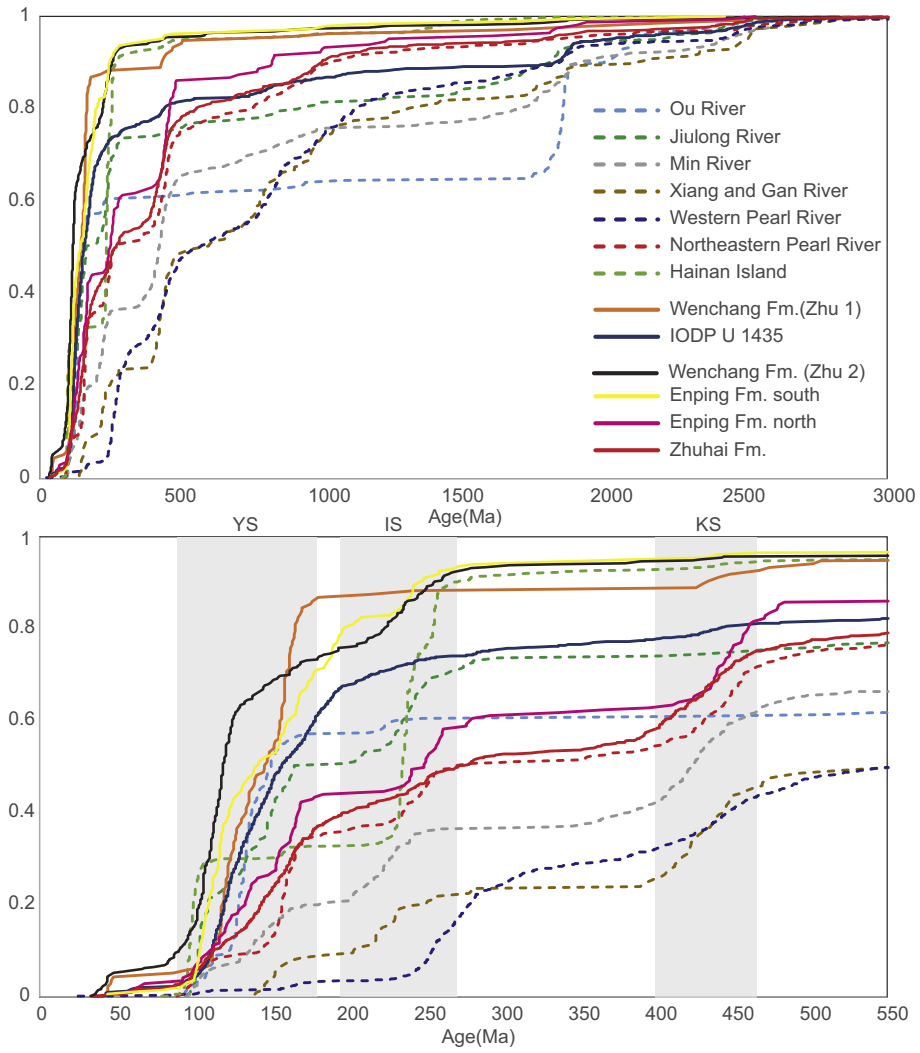

Fig. 9. Cumulative probability plots for the zircon U—Pb ages of river sands from the Cathaysia Block and from this study.

are reflected the age clusters and peaks in the kernel density estimation (Fig. 11). For the river systems, three main ages clusters of 180–150 Ma, 145–125 Ma, and 110–90 Ma are present. The Ou, Min, and Jiulong rivers flow from north to south across the southeast coast of China. The Ou River mainly flows through an area of late Yanshanian (140–80 Ma) igneous rocks with two age clusters of roughly 145–125 Ma and 110–90 Ma (Fig. 11A). In addition to these clusters, the Min and Jiulong rivers have a number of grains that range from 180 to 150 Ma (Fig. 11B, C) that may be sourced from sporadic Jurassic-aged plutons in the upper reaches of the rivers (Fig. 1A). The northeastern Pearl River, which flows through the interior of the CB, has a similar Jurassic-age group (190–150 Ma) that correlates well with the U—Pb ages from igneous bedrock in the Nanling terrane (Shi et al., 2011; Wang et al., 2013a). The northeastern Pearl River sample also contains a small age cluster from 110 to 90 Ma (Fig. 11D). The age spectrum for Hainan Island shows the same 110–90 Ma age cluster and a small age peak at 158 Ma (Fig. 11E).

In contrast, Fig. 11 (F–J) shows that samples from the PRMB and from IODP Site U1435 have more extensive and complex age ranges. Wang et al. (2017) noted that a 120 Ma age-peak in the Wenchang Formation may be diagnostic of intrabasinal provenance (Fig. 11F). A similar age-peak (121 Ma) was recognized in Eocene samples from IODP Site 1435 and was interpreted as representing sediment derived from local basement uplifts (Liu et al., 2017). This peak is not present in any of the river samples across the CB or Hainan Island. However, the Enping Formation samples from the southern part of the study area (Fig. 11H) contain a major cluster between 125 and 105 Ma, with a peak at 117 Ma. Similar age grains are present in the Zhuhai Formation and northern Enping Formation samples, but in far lower proportions. Thus, Cretaceous magmatism between 125 and 110 Ma may be a distinguishable feature of the basement of the PRMB and intrabasinal sediment sources.

6.2. Influence of basin architecture on provenance

Recent investigations of Paleogene basin-fill in the Zhu 1 depression suggest that the Wenchang Formation there is dominated by intrabasinal sediment sources; whereas, the Enping Formation is characterized by detrital zircon age signatures more characteristic of extrabasinal sources in the CB (Wang et al., 2017). Although extrabasinal influence from the CB is clear in our northernmost samples (boreholes P27 and P33), the vast majority of the Enping Formation samples in the study area have detrital zircon age distributions similar to the Wenchang Formation in the Zhu 1 and Zhu 2 depressions (Shao et al., 2016a; Wang et al., 2017) and to Eocene samples from site IODP U1435 (Liu et al., 2017). These spatial differences in the Enping Formation suggests long-distance sediment transport from the CB, to the north, was not uniform across the basin and may have been restricted to the area of the Panyu low uplift and the northern edge of Baiyun Sag. By contrast, most of the basin continued to be principally sourced

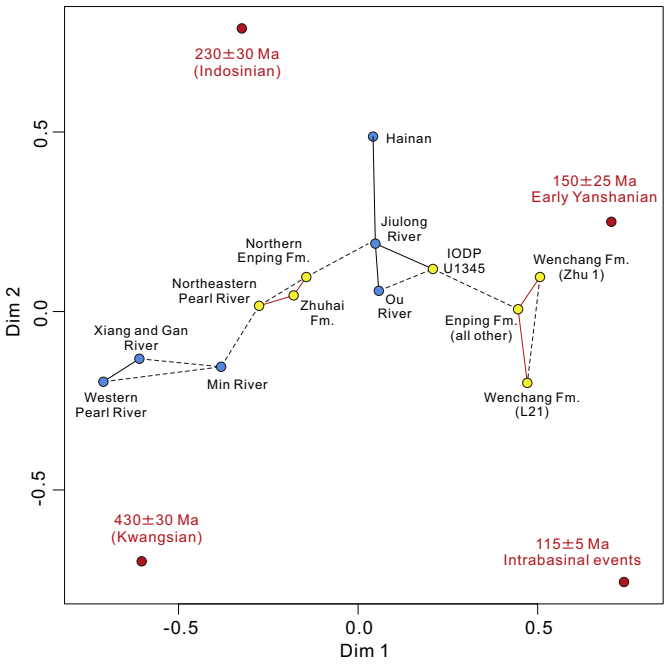

Fig. 10. Nonmetric multidimensional scaling (MDS) plot of U—Pb ages from modern river sediments (blue circles) from the CB and sedimentary strata (yellow circles) in the Pearl River Mouth Basin. Four synthetic age spectra based on 100 artificial data points with a normal distribution are also plotted (red circles) as points at 115 ± 5 Ma, representing the diagnostic age cluster of the intrabasinal basement uplifts (Wang et al., 2017), and 150 ± 25 Ma, 230 ± 30 Ma, and 430 ± 30 Ma, corresponding to the age range of the three major Phanerozoic thermal-tectonic events and associated terranes on mainland China. The plot is constructed following methods outlined in Vermeesch (2013), Vermeesch et al. (2016) and Spencer and Kirkland (2016). The stress value is 0.086, indicating goodness of the fit. (For interpretation of the references to color in this figure legend, the reader is referred to the web version of this article.)

from intrabasinal uplifts and showed little change in source-to-sink systems, a conclusion also made by Shao et al. (2016a). Such an interpretation is also consistent with the structural history of the PRMB, which suggests that Eocene to early Oligocene deposition of the Wenchang and Enping formations occurred during periods of intense rifting (Li et al., 1999; Chen et al., 2003; Clift et al., 2002).

Although long-distance sediment transport from the CB can be confidently ruled out for the Wenchang and most of the Enping Formation samples in the study area, the detrital zircon data may offer clues to a potential sediment source to west, from the Hainan Island area. The age spectra, based on the aggregated data from our study and from Shao et al. (2016a), show three Mesozoic age groups for these formations (Fig. 6C and D), corresponding to 100–110 Ma, 150–160 Ma, and 200–250 Ma. The first two age clusters correspond to the timing of episodic Yanshanian magmatism, which forms much of the basement across the central part of PRMB (Li et al., 1998; Sun et al., 2014b; Xie et al., 2014). However, the latter age peak may record the signature of an additional source area, made up of principally Indosinian (Triassic) rocks. Data compiled from rivers crossing Hainan Island to the west show a high proportion of Indosinian zircons (Fig. 6G). The Indosinian peak in the data could reflect influence from Hainan Island or similar source to the west. Although data from samples on the Yunkai uplift (boreholes B7 and B13) do not show a clear Indosinian age peak, in part because of the limited number of grains available for analysis, boreholes L13 and L21, along the southern margin of the Baiyun Sag, are characterized by a small Indosinian age peak. Data from the L21 are robust, with 367 grains making up the age distribution, providing confidence in the presence of these Indosinian-age grains.

The eastern margin of Baiyun Sag is bounded by the Dongsha uplift, which has been hypothesized to be a primary source for sediment in the basin (Shao et al., 2016a). Data from this study suggests that the uplift may have also been a barrier to sediment delivery from the CB. Detrital zircons from the Zhuhai Formation in borehole L18 have a wide age range, including a few Precambrian grains, but lack the pronounced Kwangsian peak, characteristic of extrabasinal sediment sources in the CB. Thus, the data suggest that while other parts of the basin began to receive sediment of the CB, the influence of CB sediment on the eastern margin of the Baiyun Sag was limited.

Collectively, our observations suggest that structural highs surrounding the Baiyun Sag may have served different roles during the Paleogene (Fig. 2). The Dongsha uplift in the east was both a source for sediment to the basin and barrier to sediment transported from the CB, and remained exposed until the Miocene (Li et al., 2014b); whereas, the Panyu low uplift (Fig. 2B) contains deposits of the Enping Formation, with a clear extrabasinal influence, similar to the northeastern Pearl River data, (Fig. 2B) and may have functioned as a corridor for sediment transport to the Baiyun Sag. The role of the Yunkai uplift, in the west, remains uncertain, but sediment delivery from Hainan Island or other western sources seem probable.

6.3. Tectonics, surface processes, and provenance

Results from this study and other recent provenance studies in the South China Sea (e.g., Shao et al., 2016a; Wang et al., 2017) suggest that basin architecture and evolution plays an important role in the erosion, dispersal, and ultimately provenance of sediments. The Wenchang and Enping formations were deposited in the middle Eocene to early Oligocene, during peak extension and rifting in the South China Sea, coincident with step-wise decreases in the convergence rate between the Pacific and Eurasian plates (Engebretson, 1985; Northrup et al., 1995; Lee and Lawver, 1995). Continental margin extension at this time was expressed by intense faulting, high subsidence rates, erosion, and volcanism across the PRMB and South China Sea (Shi et al., 2014; Wang et al., 2017). Collectively, these processes would have promoted erosion of uplifted footwalls to the major faults and related transfer and accommodation zones and capture of locally derived sediments. The more complicated architecture of the basin, with alternating topographic highs and lows, would have also obstructed or limited the development of continuous, large-scale drainage networks (Cao et al., 2018). By 32 Ma, sea-floor spreading and a large-scale transgression dominate, and intrabasinal structural highs, that were previously sources for sediment, were minimized, submerged, and/or overwhelmed, allowing extrabasinal sediments to gradually dominate deposition.

Although intrabasinal influence on provenance is clear, results of this study also confirm that by middle Oligocene there was increasing influence from regional or extrabasinal sediment sources and processes. Our analysis supports conclusions from previous investigations that suggest that the regional sediment supply has been controlled in large part by the ancestral Pearl River system since the Oligocene (Shao et al., 2008; Zhao et al., 2015; Shao et al., 2016a; Wang et al., 2017). However, the scale of this river system and its catchment has evolved over time. Studies based on geochemical and Nd isotopic data in the South China Sea have revealed a pronounced shift within Upper Oligocene strata that has been attributed to catchment expansion to the western plateau of Pearl River, associated with the uplift of Tibet (Shao et al., 2008, 2016b). These studies suggest that the Pearl River evolved from a small-scale river system, confined to the coast in the early Oligocene (at the time of Enping Formation deposition), to a large-scale drainage system covering bulk of the southern China in the early Miocene (Shao et al., 2008, 2016b; Wang et al., 2017; Cao et al., 2018). The relatively high percentage of Precambrian grains in the Zhuhai Formation (borehole P33) in the north (Fig. 5) may be indicative of these drainage expansions to the west and the inclusion of sediments derived from the Yangtze Block. However, the timing of uplift of SE Tibet is controversial and may have occurred as early as the Eocene (e.g., Hoke et al., 2014; Li et al., 2015; Linnemann et al., 2017). Earlier uplift would suggest that there are time lags between surface uplift, drainage

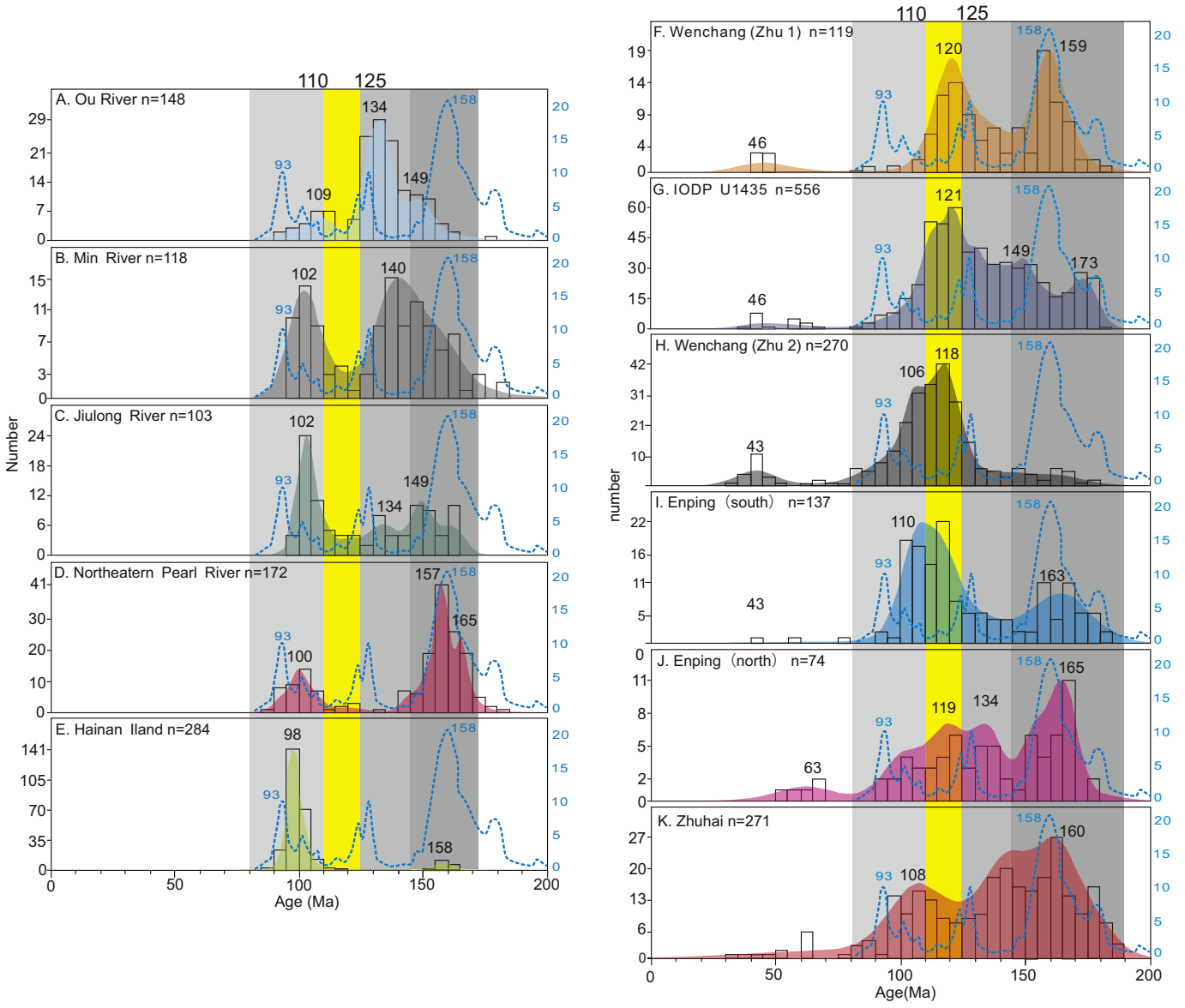

Fig. 11. Kernel density estimation (Vermeesch, 2012) and histogram (10 Ma bins) plots for Yanshanian (180–80 Ma) and younger zircons from the modern river sediment from potential source areas and samples from the Pearl River Mouth Basin. Data are from this study and the same references as in Fig. 6. The green curve shows the frequency of zircon U—Pb crystallization ages for Yanshanian granitoids in the eastern South China Block (Wang et al., 2013a). (For interpretation of the references to color in this figure legend, the reader is referred to the web version of this article.)

reorganization, and deposition. Therefore, surface uplift and related drainage expansions may be long-running processes that eventually increase drainage areas and sediment supply, and may also be responsible for the transition from intrabasinal to extrabasinal sediment sources preserved in sedimentary records.

In summary, the transition from intrabasinal to extrabasinal sediment sources recognized, in large part, between the Enping and Zhuhai formations is a consequence of a complex set of processes within the basin and within the regional provenance area. The transition was driven by both increasing extrabasinal sediment supply and the decreasing role of intrabasinal sediment sources, which are ultimately interrelated and fundamentally controlled by the regional tectonics and major sea-level changes in this period.

Based on the analysis above, we propose the following three-phase tectono-stratigraphic evolution for the central and southern PRMB: (1) In the middle Eocene, deposition of the Wenchang Formation initiates. At this time of intense rifting, the PRMB is characterized by alternating structural highs and lows. Structural highs, made up by the footwalls of the major normal faults, provided the bulk of the sediment deposited in the basins, and in some cases, impeded detritus entering from outside the basin. Strata, from the Zhu 1 depression in the north to IODP site U1435 in the south, was principally sourced from these intrabasinal sediment sources, in large part made up of 110–125 Ma magmatic rocks (Fig. 12A). (2) In the late Eocene to early Oligocene, deposition of the Enping Formation initiates. Although extension is still active, it is less intense and when paired with drainage reorganizations on the mainland associated with the uplift of Tibet allow sediments from the CB to the north to enter the PRMB (Wang et al., 2017) and reach as far as the Panyu low uplift and north slope of Baiyun Sag. Areas to south, however, were still dominated by fan deltas with intrabasinal provenance (Fig. 12B). (3) In the late Oligocene, the Zhuhai Formation develops, with sediment from the CB to north covering the bulk of the study area and reaching the southern PRMB (Fig. 12C). Considering background changes in tectonics and eustasy, the long-distance and large-scale sediment transport may have been triggered initially by uplift of Tibet and later by the initiation of sea-floor spreading and a transgression in sea-level in the South China Sea (Li et al., 2014a; Shi et al., 2014). As many of the previous structural highs became submerged,

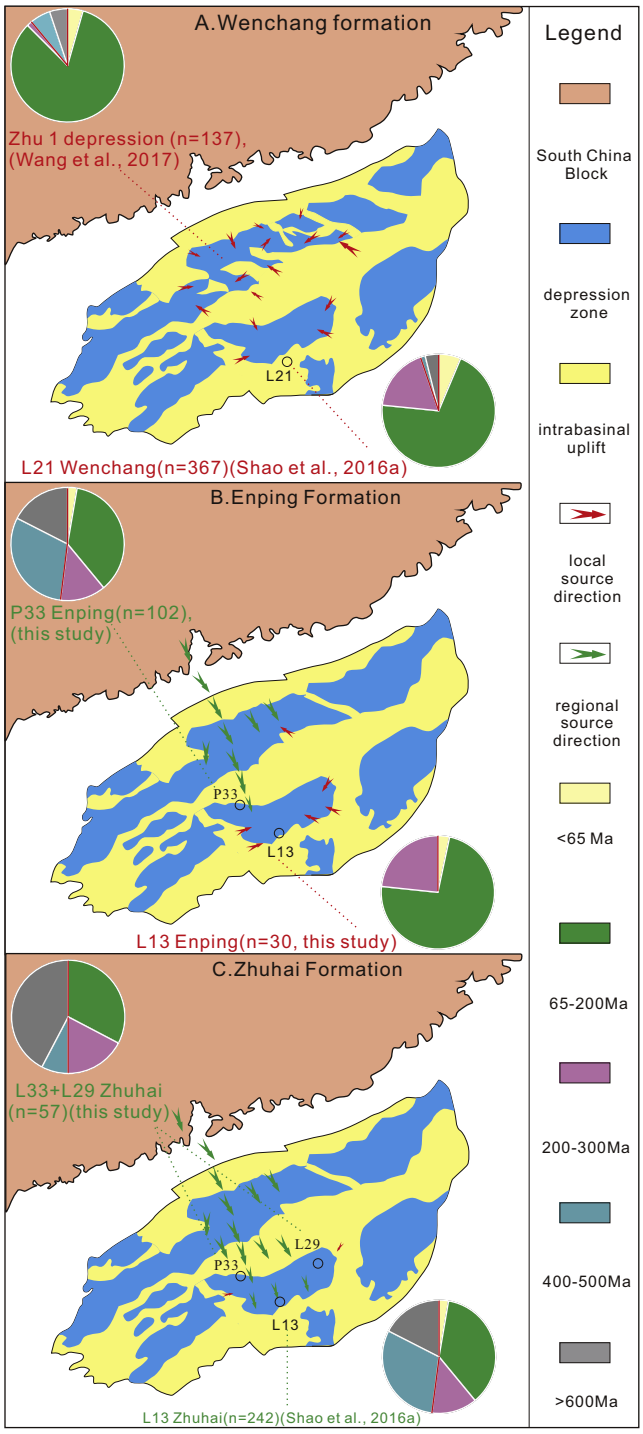

Fig. 12. Schematic diagram illustrating the Paleocene provenance evolution of the PRMB, with age pie charts from representative samples in different parts of the basin showing the spatial and temporal changes in age components. Colored arrows show local (red) versus regional (green) sources. Arrow lengths correspond to their relative contributions to the detrital zircon age signatures. (For interpretation of the references to color in this figure legend, the reader is referred to the web version of this article.)

they lost their provenance effect. However, the Dongsha uplift continued to block sediment, limiting the influence of CB sediment on the eastern margin of the Baiyun Sag until the Miocene.

7. Conclusion

In this study, we report new detrital zircon U—Pb ages from the Paleogene formations in the Baiyun Sag, Zhu 2 depression, south-central PRMB. Using published detrital zircon data from modern sediment from rivers across the CB and Hainan Island, which aid in defining potential source regions, we draw several important conclusions.

(1) Most of the late Eocene to early Oligocene Enping Formation samples are dominated by Mesozoic zircon grains and have age distributions that match the Eocene Wenchang Formation, suggesting little change in provenance during deposition of these intervals. The zircon age spectra for these samples include a peak at ~120 Ma that does not match grain ages from the CB and may be characteristic of intrabasinal sediment sources associated with Yanshanian magmatism.
(2) Spatial analysis of samples shows that the Enping Formation in the northern part of the study area has a unique source when compared to the other Late Eocene to early Oligocene samples. The data suggest that sediment delivered from the CB, where the northeastern Pearl River is located, reached as far as the Panyu low uplift, on the northern margin of Baiyun Sag, while sediments in other parts of the study area remained principally derived from intrabasinal sources.
(3) The detrital zircon age signature of the late Oligocene Zhuhai Formation, which shows an increase in the number of Paleozoic and Precambrian grains across the Baiyun Sag, is indicative of a major change in the provenance, likely associated with long-distance sediment transport from extrabasinal sources in the CB.
(4) Structural highs surrounding the Baiyun Sag served different roles during the Paleogene, operating as sources for sediment, corridors for sediment transported to the basin, or as barriers for sediment delivered from extrabasinal sources.
(5) Compiled detrital zircon data from modern rivers can properly account for intrablock heterogeneities across the CB and are easily compared with data from Paleogene strata in the PRMB, providing confidence in relationships between samples and source regions.

Supplementary data to this article can be found online at https://doi.org/10.1016/j.sedgeo.2019.04.004.

Data Availability

The data used are listed in the references, tables, and data supplements. The full suite of data is also available through the IEDA (Interdisciplinary Earth Data Alliance) EarthChem Library (www.earthchem.org) at https://doi.org/10.1594/IEDA/111268.

Acknowledgements

This study was supported by the National Science and Technology Major Projects of China (Grant No. 2016ZX05024-002-003, 2016ZX05027-001-005 and 2017ZX05032-001-004) and the China Scholarship Council. We appreciate the positive cooperation with the Beijing Research Institute of the China National Offshore Oil Corporation and technical support from State Key Laboratory of Geological Processes and Mineral Resources.

References

Andersen, T., 2005. Detrital zircons as tracers of sedimentary provenance: limiting conditions from statistics and numerical simulation. Chem. Geol. 216 (3–4), 249–270.
Cao, L., Jiang, T., Wang, Z., Zhang, Y., Sun, H., 2015. Provenance of Upper Miocene sediments in the Yinggehai and Qiongdongnan basins, northwestern South China Sea: evidence from REE, heavy minerals and zircon U–Pb ages. Mar. Geol. 361, 136–146.
Cao, L., Shao, L., Qiao, P., Zhao, Z., van Hinsbergen, D.J., 2018. Early Miocene birth of modern Pearl River recorded low-relief, high-elevation surface formation of SE Tibetan Plateau. Earth Planet. Sci. Lett. 496, 120–131.
Chen, C.M., Shi, H.S., Xu, S.C., 2003. Tertiary Hydrocarbon Reservoir Forming Conditions in the Eastern Pearl River Mouth Basin. (in Chinese). Science Press, Beijing, pp. 13–90.

Clift, P., Lin, J., 2001. Preferential mantle lithospheric extension under the South China margin. Mar. Pet. Geol. 18, 929–945. https://doi.org/10.1016/S0264-8172(01)00037-X.
Clift, P., Lee, J.I., Clark, M.K., Blusztajn, J., 2002. Erosional response of South China to arc rifting and monsoonal strengthening; a record from the South China Sea. Mar. Geol. 184, 207–226. https://doi.org/10.1016/S0025-3227(01)00301-2.
Clift, P.D., Blusztajn, J., Nguyen, A.D., 2006. Large-scale drainage capture and surface uplift in eastern Tibet-SW China before 24 Ma inferred from sediments of the Hanoi Basin, Vietnam. Geophys. Res. Lett. 33 (L19403). https://doi.org/10.1029/2006GL027772.
Clift, P.D., Long, H.V., Hinton, R., Ellam, R.M., Hannigan, R., Tan, M.T., Blusztajn, J., Duc, N.A., 2008. Evolving East Asian river systems reconstructed by trace element and Pb and Nd isotope variations in modern and ancient Red River-Song Hong sediments. Geochem. Geophys. Geosyst. 9 (4). https://doi.org/10.1029/2007GC001867.
Compston, W., Williams, I.S., Kirschvink, J.L., Zichao, Z., Guogan, M.A., 1992. Zircon U-Pb ages for the Early Cambrian time-scale. J. Geol. Soc. 149, 171–184. https://doi.org/10.1144/gsjgs.149.2.0171.
Deng, K., Yang, S., Li, C., Su, N., Bi, L., Chang, Y.P., Chang, S.C., 2017. Detrital zircon geochronology of river sands from Taiwan: Implications for sedimentary provenance of Taiwan and its source link with the East China mainland. Earth Sci. Rev. 164, 31–47.
Engebretson, D.C., 1985. Relative motions between oceanic and continental plates in the Pacific Basin. In: Engebretson, D.C., Cox, A., Gordon, R.G. (Eds.), Geological Society of America Special Papers vol. 206. Geological Society of America, Boulder, CO, pp. 1–59.
Fu, N., Deng, Y., Zhang, G., Li, Y., 2010. Transitional source rock and its contribution to hydrocarbon accumulation in superimpose rift-subsidence basin of northern South China Sea: taking Baiyun Sag of Zhu II depression as an example. Acta Pet. Sin. 31, 559–565 (in Chinese with English abstract).
Gehrels, G., 2011. Detrital Zircon U-Pb Geochronology: Current Methods and New Opportunities. In: Busby, C., Azor, A. (Eds.), Tectonics of Sedimentary Basins: Recent Advances, pp. 45–62.
He, M., Zheng, H., Clift, P.D., 2013. Zircon U–Pb geochronology and Hf isotope data from the Yangtze River sands: implications for major magmatic events and crustal evolution in Central China. Chem. Geol. 360, 186–203.
Hoke, G.D., Liu-Zeng, J., Hren, M.T., Wissink, G.K., Garzione, C.N., 2014. Stable isotopes reveal high southeast Tibetan Plateau margin since the Paleogene. Earth Planet. Sci. Lett. 394, 270–278.
Horstwood, M.S., Košler, J., Gehrels, G., Jackson, S.E., McLean, N.M., Paton, C., Pearson, N.J., Sircombe, K., Sylvester, P., Vermeesch, P., Bowring, J.F., 2016. Community-derived standards for LA-ICP-MS U-(Th-) Pb geochronology—uncertainty propagation, age interpretation and data reporting. Geostand. Geoanal. Res. 40 (3), 311–332.
Huang, C., Zhou, D., Sun, Z., Chen, C., Hao, H., 2005. Deep crustal structure of Baiyun Sag, northern South China Sea revealed from deep seismic reflection profile. Chin. Sci. Bull. 50, 1131–1138. https://doi.org/10.1360/04wd0207.
Jackson, S.E., Pearson, N.J., Griffin, W.L., Belousova, E.A., 2004. The application of laser ablation-inductively coupled plasma-mass spectrometry to in situ U–Pb zircon geochronology. Chem. Geol. 211 (1–2), 47–69.
Jiang, T., Cao, L., Xie, X., Wang, Z., Li, X., Zhang, Y., Zhang, D., Sun, H., 2015. Insights from heavy minerals and zircon U–Pb ages into the middle Miocene–Pliocene provenance evolution of the Yinggehai Basin, northwestern South China Sea. Sediment. Geol. 327, 32–42.
Košler, J., Sláma, J., Belousova, E., Corfu, F., Gehrels, G.E., Gerdes, A., Horstwood, M.S., Sircombe, K.N., Sylvester, P.J., Tiepolo, M., Whitehouse, M.J., 2013. U-Pb detrital zircon analysis—results of an inter-laboratory comparison. Geostand. Geoanal. Res. 37 (3), 243–259.
Lee, T.Y., Lawver, L.A., 1995. Cenozoic plate reconstruction of Southeast Asia. Tectonophysics 251 (1), 85–138.
Li, P.L., 1993. Cenozoic structural movement of Pearl River Mouth Basin. China Offshore Oil Gas 7 (6), 11–17 (in Chinese with English abstract).
Li, X.H., 2000. Cretaceous magmatism and lithospheric extension in Southeast China. J. Asian Earth Sci. 18, 293–305. https://doi.org/10.1016/S1367-9120(99)00060-7.
Li, P., Liang, H., Dai, Y., 1998. Exploration perspective of basement hydrocarbon accumulations in the Pearl River Mouth Basin. China Offshore Oil Gas (Geology) 12, 361–369 (in Chinese with English abstract).
Li, S., Lin, C., Zhang, Q., Yang, S., Wu, P., 1999. Episodic rifting of continental marginal basins and tectonic events since 10 Ma in the South China Sea. Chin. Sci. Bull. 44, 10–23. https://doi.org/10.1007/BF03182877.
Li, C.F., Xu, X., Lin, J., Sun, Z., Zhu, J., Yao, Y., Zhao, X., Liu, Q., Kulhanek, D.K., Wang, J., Song, T., 2014a. Ages and magnetic structures of the South China Sea constrained by deep tow magnetic surveys and IODP Expedition 349. Geochem. Geophys. Geosyst. 15, 4958–4983. https://doi.org/10.1002/2014GC005567.
Li, X., Shi, H., Du, J., Chen, S., Zhang, C., Yu, Y., 2014b. Capability of Dongsha Massif as provenance during Zhuhai-Zhujiang Formations. Acta Pet. Sin. 32, 654–662 (in Chinese with English abstract).
Li, S., Currie, B.S., Rowley, D.B., Ingalls, M., 2015. Cenozoic paleoaltimetry of the SE margin of the Tibetan Plateau: constraints on the tectonic evolution of the region. Earth Planet. Sci. Lett. 432, 415–424.
Linnemann, U., Su, T., Kunzmann, L., Spicer, R.A., Ding, W.N., Spicer, T.E.V., Zieger, J., Hofmann, M., Moraweck, K., Gärtner, A., Gerdes, A., Marko, L., Zhang, S.T., Li, S.F., Tang, H., Huang, J., Mulch, A., Mosbrugger, V., Zhou, Z.K., 2017. New U–Pb dates show a Paleogene origin for the modern Asian biodiversity hot spots. Geology 46, 3–6.
Liu, Y., Hu, Z., Gao, S., Günther, D., Xu, J., Gao, C., Chen, H., 2008. In situ analysis of major and trace elements of anhydrous minerals by LA-ICP-MS without applying an internal standard. Chem. Geol. 257, 34–43. https://doi.org/10.1016/j.chemgeo.2008.08.004.
Liu, Y., Gao, S., Hu, Z., Gao, C., Zong, K., Wang, D., 2010a. Continental and oceanic crust recycling-induced melt–peridotite interactions in the Trans-North China Orogen: U–Pb dating, Hf isotopes and trace elements in zircons from mantle xenoliths. J. Petrol. 51, 537–571. https://doi.org/10.1093/petrology/egp082.
Liu, Y., Hu, Z., Zong, K., Gao, C., Gao, S., Xu, J., Chen, H., 2010b. Reappraisement and refinement of zircon U-Pb isotope and trace element analyses by LA-ICP-MS. Chin. Sci. Bull. 55, 1535–1546. https://doi.org/10.1007/s11434-010-3052-4.
Liu, C., Clift, P.D., Carter, A., Böning, P., Hu, Z., Sun, Z., Pahnke, K., 2017. Controls on modern erosion and the development of the Pearl River drainage in the late Paleogene. Mar. Geol. 394, 52–68.
Malusà, M.G., Carter, A., Limoncelli, M., Villa, I.M., Garzanti, E., 2013. Bias in detrital zircon geochronology and thermochronometry. Chem. Geol. 359 (6), 90–107. https://doi.org/10.1016/j.chemgeo.2013.09.016.
Malusà, M.G., Resentini, A., Garzanti, E., 2016. Hydraulic sorting and mineral fertility bias in detrital geochronology. Gondwana Res. 31, 1–19. https://doi.org/10.1016/j.gr.2015.09.002.
Northrup, C.J., Royden, L.H., Burchfiel, B.C., 1995. Motion of the Pacific plate relative to Eurasia and its potential relation to Cenozoic extension along the eastern margin of Eurasia. Geology 23 (8), 719–722. https://doi.org/10.1130/0091-7613(1995)023%3C0719:MOTPPR%3E2.3.CO;2.
Pang, X., Yang, S., Zhu, M., Li, J.S., 2004. Deep-water fan systems and petroleum resources on the northern slope of the South China Sea. Acta Geol. Sin. 78 (3), 626–631.
Pang, X., Chen, C.M., Wu, M.S., He, M., Wu, X.J., 2006. The Pearl River deep-water fan systems and significant geological events. Adv. Earth Science 21 (8), 23–29 (in Chinese with English abstract).
Pang, X., Chen, C., Zhu, M., He, M., Shen, J., Lian, S., Wu, X., Shao, L., 2009. Baiyun movement: a significant tectonic event on Oligocene/Miocene boundary in the northern South China Sea and its regional implications. J. Earth Sci. 20, 49–56.
Peltzer, G., Tapponnier, P., 1988. Formation and evolution of strike-slip faults, rifts, and basins during the India-Asia collision: an experimental approach. J. Geophys. Res. Solid Earth 93 (B12), 15085–15117.
Ru, K., Pigott, J.D., 1986. Episodic rifting and subsidence in the South China Sea. AAPG Bull. 70, 1136–1155.
Shao, L., Pang, X., Chen, C., Shi, H., Li, Q., Qiao, P., 2008. Late Oligocene sedimentary environments and provenance abrupt change event in the northern South China Sea. Front. Earth Sci. China 2 (2), 138–146. https://doi.org/10.1007/s11707-008-0041-x.
Shao, L., Cao, L., Pang, X., Jiang, T., Qiao, P., Zhao, M., 2016a. Detrital zircon provenance of the Paleogene syn-rift sediments in the northern South China Sea. Geochem. Geophys. Geosyst. 17, 255–269. https://doi.org/10.1002/2015GC006113.
Shao, L., Qiao, P., Zhao, M., Li, Q., Wu, M., Pang, X., Zhang, H., 2016b. Depositional characteristics of the northern South China Sea in response to the evolution of the Pearl River. Geol. Soc. Lond. Spec. Publ. 429 (6), 31–44. https://doi.org/10.1144/SP429.2.
Shi, H.S., Xu, C.H., Zhou, Z.Y., Ma, C.Q., 2011. Zircon U-Pb dating on granitoids from the northern South China Sea and its geotectonic relevance. Acta Geol. Sin. 85, 1359–1372.
Shi, H., He, M., Zhang, L., Yu, Q., Pang, X., Zhong, Z., Liu, L., 2014. Hydrocarbon geology, accumulation pattern and the next exploration strategy in the eastern Pearl River Mouth Basin. China Offshore Oil Gas 26, 11–22 (in Chinese with English abstract).
Spencer, C.J., Kirkland, C.L., 2016. Visualizing the sedimentary response through the orogenic cycle: a multidimensional scaling approach. Lithosphere 8 (1), 29–37.
Spencer, C.J., Kirkland, C.L., Taylor, R.J., 2016. Strategies towards statistically robust interpretations of in situ U–Pb zircon geochronology. Geosci. Front. 7 (4), 581–589.
Spencer, C.J., Yakymchuk, C., Ghaznavi, M., 2017. Visualising data distributions with kernel density estimation and reduced chi-squared statistic. Geosci. Front. 8 (6), 1247–1252.
Sun, Z., Xu, Z., Sun, L., Pang, X., Yan, C., Li, Y., 2014a. The mechanism of post-rift fault activities in Baiyun Sag, Pearl River Mouth Basin. J. Asian Earth Sci. 89 (3), 76–87.
Sun, X., Zhang, X., Zhang, G., Lu, B., Yue, J., Zhang, B., 2014b. Texture and tectonic attribute of Cenozoic basin basement in the northern South China Sea. Sci. China Earth Sci. 57, 1199–1211. https://doi.org/10.1007/s11430-014-4835-2.
Vermeesch, P., 2004. How many grains are needed for a provenance study? Earth Planet. Sci. Lett. 224 (3–4), 441–451.
Vermeesch, P., 2012. On the visualisation of detrital age distributions. Chem. Geol. 312-313, 190–194. https://doi.org/10.1016/j.chemgeo.2012.04.021.
Vermeesch, P., 2013. Multi-sample comparison of detrital age distributions. Chem. Geol. 341, 140–146. https://doi.org/10.1016/j.chemgeo.2013.01.010.
Vermeesch, P., Resentini, A., Garzanti, E., 2016. An R package for statistical provenance analysis. Sediment. Geol. 336, 14–25. https://doi.org/10.1016/j.sedgeo.2016.01.009.
Wang, Y., Fan, W., Zhang, G., Zhang, Y., 2013a. Phanerozoic tectonics of the South China Block: key observations and controversies. Gondwana Res. 23, 1273–1305. https://doi.org/10.1016/j.gr.2012.02.019.
Wang, J., Pang, X., Tang, D., Liu, B., Xu, D., 2013b. Transtensional tectonism and its effects on the distribution of sand bodies in the Paleogene Baiyun Sag, Pearl River Mouth Basin, China. Mar. Geophys. Res. 34 (3–4), 195–207.
Wang, C., Liang, X., Zhou, Y., Fu, J., Jiang, Y., Dong, C., Xie, Y., Tong, C., Pei, J., Liu, P., 2015. Construction of age frequences of provenances on the eastern side of the Yinggehai Basin: studies on LA-ICP-MS U-Pb ages of detrital zircons from six modern rivers, Western Hainan, China. Earth Sci. Front. 22, 277–289. https://doi.org/10.13745/j.esf.2015.04.028 (in Chinese with English abstract).
Wang, W., Ye, J., Bidgoli, T., Yang, X., Shi, H., Shu, Y., 2017. Using detrital zircon geochronology to constrain Paleogene provenance and its relationship to rifting in the Zhu 1 Depression, Pearl River Mouth Basin, South China Sea. Geochem. Geophys. Geosyst. 18 (11), 3976–3999. https://doi.org/10.1002/2017GC007110.
Wu, Z., Zhu, W., Shao, L., Xu, C., 2016. Sedimentary facies and the rifting process during the late Cretaceous to early Oligocene in the northern continental margin, South China Sea. Interpretation 4, SP33–SP45.
Xie, H., Zhou, D., Li, Y., Pang, X., Li, P., Chen, G., Li, F., Cao, J., 2014. Cenozoic tectonic subsidence in deepwater sags in the Pearl River Mouth Basin, northern South China Sea. Tectonophysics 615, 182–198.

Xu, X., O'Reilly, S.Y., Griffin, W.L., Wang, X., Pearson, N.J., He, Z., 2007. The crust of Cathaysia: age, assembly and reworking of two terranes. Precambrian Res. 158, 51–78. https://doi.org/10.1016/j.precamres.2007.04.010.

Xu, Y., Sun, Q., Yi, L., Yin, X., Wang, A., Li, Y., Chen, J., 2014a. Detrital zircons U-Pb age and Hf isotope from the western side of the Taiwan Strait: implications for sediment provenance and crustal evolution of the northeast Cathaysia Block. Terr. Atmos. Ocean. Sci. 25 (4), 506–535.

Xu, Y., Sun, Q., Cai, G., Yin, X., Chen, J., 2014b. The U–Pb ages and Hf isotopes of detrital zircons from Hainan Island, South China: implications for sediment provenance and the crustal evolution. Environ. Earth Sci. 71, 1619–1628. https://doi.org/10.1007/s12665-013-2566-x.

Xu, Y., Wang, C.Y., Zhao, T., 2016. Using detrital zircons from river sands to constrain major tectono-thermal events of the Cathaysia Block, SE China. J. Asian Earth Sci. 124, 1–13. https://doi.org/10.1016/j.jseaes.2016.04.012.

Yu, J.H., O'Reilly, S.Y., Wang, L., Griffin, W.L., Zhou, M.F., Zhang, M., Shu, L., 2010. Components and episodic growth of Precambrian crust in the Cathaysia Block, South China: evidence from U–Pb ages and Hf isotopes of zircons in Neoproterozoic sediments. Precambrian Res. 181, 97–114.

Yu, J.H., O'Reilly, S.Y., Zhou, M.F., Griffin, W.L., Wang, L., 2012. U–Pb geochronology and Hf–Nd isotopic geochemistry of the Badu Complex, Southeastern China: implications for the Precambrian crustal evolution and paleogeography of the Cathaysia Block. Precambrian Res. 222, 424–449.

Zeng, Z., Yang, X., Zhu, H., Xia, C., Niu, X., Chen, Y., 2017. Development characteristics and significance of large delta of upper Enping Formation, Baiyun Sag. Earth Sci. 42 (1), 78–92 (in Chinese with English abstract).

Zhang, G., Yang, H., Ying, C., Mo, J., Ke, W., Yang, D., 2014. The Baiyun Sag: a giant rich gas-generation sag in the deepwater area of the Pearl River Mouth basin. Nat. Gas Ind. 34 (11), 11–25 (in Chinese with English abstract).

Zhang, X., Huang, C., Wang, Y., Clift, P.D., Yan, Y., Fu, X., Chen, D., 2017. Evolving Yangtze River reconstructed by detrital zircon U-Pb dating and petrographic analysis of Miocene marginal sea sedimentary rocks of the Western Foothills and Hengchun Peninsula, Taiwan. Tectonics 36. https://doi.org/10.1002/2016TC004357.

Zhao, M., Shao, L., Qiao, P., 2015. Characteristics of detrital zircon U-Pb geochronology of the Pearl River Sands and its implication on provenances. J. Tongji Univ. (Nat. Sci.) 43, 89–97. https://doi.org/10.11908/j.issn.0253-374x.2015.06.018 (in Chinese with English abstract).

Zheng, H., Clift, P.D., Wang, P., Tada, R., Jia, J., He, M., Jourdan, F., 2013. Pre-Miocene birth of the Yangtze River. Proc. Natl. Acad. Sci. 110 (19), 7556–7561. https://doi.org/10.1073/pnas.1216241110.

Zhou, X.M., Li, W.X., 2000. Origin of Late Mesozoic igneous rocks in Southeastern China: implications for lithosphere subduction and underplating of mafic magmas. Tectonophysics 326, 269–287. https://doi.org/10.1016/S0040-1951(00)00120-7.

Zhou, X.M., Sun, T., Shen, W.Z., Shu, L.S., Niu, Y.L., 2006. Petrogenesis of Mesozoic granitoids and volcanic rocks in South China: a response to tectonic evolution. Episodes 29, 26–33.